TECHNICAL NOTE

D-746

FLIGHT CONTROLLABILITY LIMITS AND RELATED HUMAN TRANSFER FUNCTIONS AS DETERMINED FROM SIMULATOR AND FLIGHT TESTS

By Lawrence W. Taylor, Jr., and Richard E. Day

Flight Research Center
Edwards, Calif.

NATIONAL AERONAUTICS AND SPACE ADMINISTRATION
WASHINGTON
May 1961

NATIONAL AERONAUTICS AND SPACE ADMINISTRATION

TECHNICAL NOTE D-746

FLIGHT CONTROLLABILITY LIMITS AND RELATED HUMAN TRANSFER FUNCTIONS AS DETERMINED FROM SIMULATOR AND FLIGHT TESTS

By Lawrence W. Taylor, Jr., and Richard E. Day

SUMMARY

A simulator study and flight tests were performed to determine the levels of static stability and damping necessary to enable a pilot to control the longitudinal and lateral-directional dynamics of a vehicle for short periods of time. Although a basic set of aerodynamic characteristics was used, the study was conducted so that the results would be applicable to a wide range of flight conditions and configurations. Novel piloting techniques were found which enabled the pilot to control the vehicle at conditions that were otherwise uncontrollable. The influence of several critical factors in altering the controllability limits was also investigated.

Several human transfer functions were used which gave fairly good representations of the controllability limits determined experimentally for the short-period longitudinal, directional, and lateral modes. A transfer function with approximately the same gain and phase angle as the pilot at the controlling frequencies along the controllability limits was also derived.

INTRODUCTION

In the design of future flight vehicles, it may be necessary to accept marginal levels of static stability or damping, or both, of the basic airframe. Satisfactory vehicle characteristics will, of necessity, be obtained through stability-augmentation systems. For conditions of stability-augmentation failure, however, it becomes of the utmost importance to understand the flight-control problem in marginally controllable regions to determine if the pilot can cope with the emergency condition.

Previous work in the field of controllability (ref. 1, for example) was largely concerned with configurations which are termed "unacceptable"

for normal flight. These configurations did not, in general, approach the limiting conditions beyond which it is impossible for the pilot to maintain control. An early attempt to define these more extreme controllability limits is reported in reference 2; however, these tests were restricted to a simple swiveling chair having only one degree of freedom with variable dynamic characteristics.

In an effort to determine the controllability limits for conditions more closely approximating actual flight, a five-degree-of-freedom fixed-base-simulator study was conducted at the NASA Flight Research Center, Edwards, Calif. This study permitted systematic variations of the static stability and damping in both the longitudinal and lateral-directional modes. In addition, the effects of other factors such as piloting technique, learning, and distractions were investigated to determine their influence on the controllability limits. This paper summarizes and compares the results of this study with limited flight data from variable-stability airplanes and with data from the human centrifuge of the Naval Air Development Center, Johnsville, Pa. (ref. 3). The flight controllability limits determined in these investigations are used in this paper to study human transfer functions which might be applied to similar marginally controllable tasks.

SYMBOLS

B	basic value of a dimensional derivative as listed in table I
b	wing span, ft
C_n	yawing-moment coefficient
g	acceleration due to gravity, 32.2 ft/sec^2
I_X	moment of inertia about the principal X-axis, slug-ft^2
I_Y	moment of inertia about the principal Y-axis, slug-ft^2
I_Z	moment of inertia about the principal Z-axis, slug-ft^2
$I_{X_e}p_e$	angular momentum of the engines, slug-ft^2/sec
K	pilot gain
$K_1 \ldots K_5$	general coefficient

L	$\frac{\text{Rolling moment}}{I_X}$, per sec^2
M	$\frac{\text{Pitching moment}}{I_Y}$, per sec^2
m	mass, slugs
N	$\frac{\text{Yawing moment}}{I_Z}$, per sec^2
P	period, sec
p	roll rate, radians/sec
q	pitch rate, radians/sec
r	yaw rate, radians/sec
S	wing area, sq ft
s	Laplace transform variable
T_I	lag time constant, sec
T_L	lead time constant, sec
T_N	neuromuscular lag time constant, sec
T_2	time to double amplitude of the envelope of an oscillatory response, sec
T'_2	time to double amplitude of purely divergent response due to a negligible disturbance, sec
t	time, sec
V	velocity, ft/ sec
Y	$\frac{\text{Side force}}{mV}$, per sec

Z	$\frac{\text{Normal force}}{mV}$, per sec
α	angle of attack, radians
α_0	trim angle of attack of the principal axis at zero roll rate, radians
β	angle of sideslip, radians
Δ	incremental change
δ_a	aileron deflection (left aileron down is positive), radians
δ_e	elevator deflection (trailing edge down is positive), radians
δ_r	rudder deflection (trailing edge left is positive), radians
ζ	damping ratio
ζ_θ	damping ratio of the short-period longitudinal mode
$2\zeta\omega_n$	damping of the short-period mode (see appendix A)
$2\zeta_\theta\omega_{n_\theta}$	damping of the short-period longitudinal mode
$2\zeta_\psi\omega_{n_\psi}$	damping of the short-period (Dutch roll) lateral-directional mode
θ	pitch angle, radians
τ	reaction time delay, sec
τ_φ	time constant in roll, sec
φ	bank angle, phase angle, radians or deg
ω	frequency, radians/sec
ω_n	undamped natural frequency, radians/sec
ω_n^2	static stability of the short-period mode (see appendix A)

ω_{n_θ} undamped natural frequency of the short-period longitudinal mode, radians/sec

$\omega_{n_\theta}^2$ static stability of the short-period longitudinal mode

$\omega_{n_\psi}^2$ static stability of the short-period (Dutch roll) lateral-directional mode

Subscripts:

max maximum

The subscripts p, q, r, α, β, δ_a, δ_e, and δ_r indicate the partial derivative with respect to the specific subscript; that is, $N_{\delta_a} = \frac{\partial N}{\partial \delta_a} = \frac{qSb}{I_Z} C_{n_{\delta_a}}$ and is the yawing "moment" due to aileron deflection. A dot above a variable indicates that the variable is a time derivative.

The following notations indicate the piloting technique employed:

($\delta_a \sim \varphi$) ailerons used in the normal manner to control bank angle

($\delta_a \sim \beta$) ailerons used as rudders to control sideslip

($\delta_a \sim \beta \sim \varphi$) ailerons used as a rudder to control sideslip, and sideslipping purposely to control bank angle

($\delta_a \sim \varphi \sim \beta$) ailerons used to control bank, and banking purposely to control sideslip

($\delta_r \sim \beta$) rudder used in normal manner to control sideslip

($\delta_r \sim \beta \sim \varphi$) rudder used to control sideslip, and sideslipping purposely to control bank angle

SCOPE OF STUDY

As a general procedure for determining controllability limits, the pilot was assigned the task of maintaining or gradually changing the airplane attitude. The pilot controlled the airplane about all

three axes, and the levels of stability and damping of the longitudinal- or the lateral-directional modes were progressively decreased until the aircraft became uncontrollable. A condition was termed uncontrollable when the airplane excursions could not be kept within the following limits for 30 seconds:

$$\Delta\alpha < 2^\circ$$

$$\Delta\beta < 2^\circ$$

$$\Delta\varphi < 45^\circ$$

In general, it is difficult to establish the levels of stability and damping necessary for a pilot to maintain control under emergency conditions because of a number of factors, such as surprise, which cannot be readily analyzed. Under nearly ideal conditions, however, controllability boundaries are definable, and the effects of various factors on the boundaries can be determined by using the fixed-base simulator.

The primary parameters used in the following analysis to plot the controllability limits for both the longitudinal and the lateral-directional short-period modes are static stability ω_n^2 and damping $2\zeta\omega_n$. These parameters characteristically appear in the denominator of the control transfer functions (see appendix A) and were chosen because of their significant relationship to the aircraft motion even in the proximity of zero static stability. Other parameters considered had distinct disadvantages, as, for example, damping ratio ζ which approaches infinity as ω_n approaches zero. The range of static stability ω_n^2 investigated was from -25 to 100; the range of damping $2\zeta\omega_n$ was from -2 to 15.

In addition, the flight controllability limits were found for several levels of pilot learning, display interruption, and various important aerodynamic parameters. Changes in the aerodynamic parameters were made as multiples of the basic values for the generalized supersonic configuration listed in table I.

Flight test and centrifuge data were used to verify the results of the fixed-base-simulator tests. Although the data were somewhat limited in quantity, they are believed to be significant and give confidence in the conclusions of this study. A variety of human transfer functions was studied relative to the controllability limits defined by the functions.

SIMULATION

Fixed-Base Simulator

The fixed-base simulator employed a closed loop consisting of the pilot, an analog computer, and the display of the simulated aircraft's motion. The analog computer was mechanized to solve the equations of motion of the airplane for five degrees of freedom with speed invariant. The basic set of coefficients used is listed in table I. Longitudinal and lateral control were accomplished through a side-located controller, and rudder pedals were provided for directional control. Some tests were also made with a conventional center stick. The only difference observed between the tests was an increase in the amount of physical work required with the center stick. The display to the pilot consisted of a moving line on a 17-inch oscilloscope presenting angles of attack, sideslip, and bank in the manner shown in figure 1. The scales used were such that the angular displacements relative to the pilot's eyes equaled the angles of attack and sideslip. Little effect on the control task was noted whether pitch angle or angle of attack was displayed.

Test Airplanes

The flight investigations of the longitudinal and lateral-directional controllability limits were performed at the NASA Ames Research Center with a YF-86D and an F-86E airplane, respectively. The control systems of the airplanes were modified to enable the pilot to vary, in flight, the effective static stability and damping of the short-period longitudinal and lateral-directional modes. Detailed descriptions of these systems are given in references 4 and 5.

The control task for the flight-test program was similar to that for the fixed-base-simulator program and consisted of maintaining a constant airplane attitude. The flight program was contrived primarily to verify the conclusions of the simulator program and was, of necessity, much more limited in scope. The values of the simulated airplane characteristics used in the flight tests are given in table II.

Human Centrifuge

The piloting tasks performed on the human centrifuge at the Naval Air Development Center simulated the control problems anticipated for a multistage boost vehicle and emphasized the longitudinal rather than the lateral and directional modes. For the centrifuge study, the stability characteristics changed markedly with time because of the rapid variations of mass and the change of inertia and center-of-gravity location

of the boost vehicle. The levels of static stability and damping which occur immediately after staging, and represent the most severe conditions possible, were chosen for this study. In addition, the pilot was without control for a brief interval during staging. Further details of the simulation are included in reference 3.

FLIGHT CONTROLLABILITY LIMITS

In the following section the controllability limits from the fixed-base-simulator tests are presented for the longitudinal, the lateral-directional, and the coupled control modes. The limits for each mode are assessed in relation to the results from flight, human centrifuge, and other related tests. In a later section these limits are reviewed in the light of their predictability by means of human transfer functions.

Longitudinal Control

The controllability limit found for the longitudinal short-period mode is presented in figure 2. The limit approaches zero damping at a frequency of 10 radians/second and reaches a maximum level of negative damping $\left(2\zeta_{\theta}\omega_{n_{\theta}} = -1.3 \text{ or } T_2 = 1.0 \text{ sec}\right)$ at a frequency of about 4 radians/second. The limit encompasses the zero static stability and zero damping point, then follows a time to double amplitude of about 0.3 second in the purely divergent, statically unstable regime. The controllability limit was more sharply defined at frequencies below 1 cps than above. At the higher frequencies, the technique for controlling the motion was not learned as quickly by the pilot as were the techniques used for the lower frequency and the purely divergent conditions. The mean deviation of the values of damping found controllable was 0.24; the mean deviation of static stability was 1.6 on the average but was proportional to the distance from the "knee" of the controllability limit.

When controlling the high-frequency dynamic instability in the region of negative damping, the pilots applied control in sharp pulses in an effort to time and size the pulses such that $\dot{\alpha}$ would be zero as the trim angle of attack was reached. Because the pilot was never able to attain these exact conditions, he repeatedly adjusted the size of the pulse and the trim (steady) control position. The resultant continuous oscillation of varying amplitude is shown in figure 3(a). Also included in this figure is a control-fixed envelope of the motion which indicates the magnitude of the dynamic divergence that would occur if no control were applied. It should be noted that the first pulse was poorly timed, which increased the amplitude of the motion over that resulting from no input.

No pilot-induced oscillations were encountered at conditions of high frequency and low damping. Two important factors which could contribute to pilot-induced oscillations, however, were not present in the simulation: the accelerations acting upon the pilot's body, and control-system characteristics such as lag and high sensitivity at conditions of high static stability.

To control the lower-frequency dynamic instability, the pilots applied control continuously, as shown in figure 3(b). By so doing, they were able to compensate for increasing amounts of dynamic instability in terms of $2\zeta_\theta\omega_{n_\theta}$ as the frequency was decreased to about 4 radians/second. As the frequency was further reduced toward zero, the pilots were able to tolerate less dynamic instability caused by increased control sensitivity, since even small control movements resulted in large changes in the trim angle of attack. The control sensitivity used was somewhat higher than the optimum range indicated in reference 6 for this range of $\omega_{n_\theta}^2$. Lower sensitivities had no appreciable effect on the controllability limit.

Controlling the pure divergence in the region of a static instability was more natural and less tiring than controlling the oscillatory airplane motions, inasmuch as the pilot needed only to counteract the angle-of-attack divergence (fig. 3(c)) without leading the motion to stabilize the aircraft. The lower trend of the controllability limit, essentially, continues indefinitely. With large amounts of static instability it has been observed that the control problem becomes essentially first order (see appendix A), that is,

$$\frac{\alpha(s)}{\delta_e(s)} = \frac{M_{\delta_e}/\omega_{n_\theta}^2}{\frac{s^2}{\omega_{n_\theta}^2} + \frac{2\zeta_\theta s}{\omega_{n_\theta}} + 1} \approx \frac{M_{\delta_e}/\omega_{n_\theta}^2}{\frac{2\zeta_\theta s}{\omega_{n_\theta}} + 1}$$

with the gain $\frac{M_{\delta_e}}{\omega_{n_\theta}^2}$ being reduced $\left(\omega_{n_\theta}^2 \text{ rather than } M_{\delta_e} \text{ was changed}\right)$ as greater levels of instability are reached. Effective gain reductions by a factor of as much as 8 $\left(\omega_{n_\theta}^2 \text{ decreased from } -10 \text{ to } -80\right)$ failed to produce any noticeable deterioration in performance.

In general, when it was possible to keep the amplitude of the motion small, the required control motion was also small and more accurately

timed. The limit of the control available did, however, restrict the amplitude of the motion that was controllable but did not compromise controllability within the allowable amplitude of 2°.

The controllability limits are relatively insensitive to the allowable excursions used to define controllability criteria. This is especially true for statically stable conditions, as noted in figure 4. In this figure, comparisons are made between the limits for $\Delta\alpha$ of 2° (solid line) and for conditions in which control was completely lost (dashed line).

An increase in altitude from 40,000 feet to 70,000 feet had no appreciable effect on the controllability boundary, even though the control sensitivity was reduced by a factor of 5 (atmospheric-density ratio).

Under actual flight conditions it is not likely that a pilot could control a vehicle having characteristics corresponding to a point on the controllability-limit boundary. Thus, it was desirable to determine the effect of less than ideal conditions on the pilot's performance. This was simulated by interrupting the pilot's presentation for 2 seconds every 10 seconds. As shown in figure 5, this interruption reduced the pilot's ability to control unstable conditions. When interrupted, he could control only to basic conditions requiring $T_2' = 0.5$ second, as compared to $T_2' = 0.3$ second without interruption. For the dynamically unstable cases, the controllability limit changed from $T_2 = 1.0$ second to $T_2 = 1.3$ seconds when the presentation-interruption technique was used.

The effect of learning on the pilot's ability to establish controllability boundaries is shown in figure 6. The dashed line indicating the "early" limit was determined from the first few runs of several pilots. No single subject could establish the entire early-limit controllability boundary because of his rapid advance in learning to control unstable configurations. Although some pilots became proficient more quickly than others, there was no significant variation in the levels of instability which could be controlled by the different pilots, or even non-pilots, after they had become completely familiar with the task.

Correlation with motion simulators and flight tests.- A limited investigation with the YF-86D variable-stability airplane[1] of the Ames Research Center showed that even under actual flight conditions a pilot could control the large degree of static instability indicated by the fixed-base simulator (fig. 7). The pilot believed that he could control

---

[1]Additional data recently made available in NASA TN D-779 "Flight Investigation Using Variable-Stability Airplanes of Minimum Stability Requirements for High-Speed, High-Altitude Vehicles," by Norman M. McFadden, Richard M. Vomaske, and Donovan R. Heinle of the NASA Ames Research Center further validate the controllability limit established during the fixed-base-simulator investigation and have been included in figure 7.

a slightly more unstable condition, but the mechanical limit of the simulated instability was reached at the point indicated.

As a result of the failure of a rocket casing to separate from an F-100 airplane during zero-length launch tests, flight experience was obtained in controlling a statically unstable (short-period) airplane. As well as can be determined, the airplane characteristics corresponding to this flight condition are shown in figure 7 for comparison with the fixed-base controllability boundaries. The pilot controlled and maneuvered the airplane in this condition for more than 1 hour before electing to bail out rather than attempt a landing.

Also shown in figure 7 is the acceptable area determined by using a variable-stability F-94 airplane (ref. 1). A direct comparison is included to give a better understanding of the relative position of the controllability limits.

The pilot-opinion boundaries from reference 1 are compared in figure 8(a) with similar results obtained from a fixed-base simulation in reference 7. It was concluded in reference 7 that the fixed-base simulator "is obviously not realistic" for short-period frequencies above 0.6 cycle per second, but, apparently, is realistic for moderate frequencies. Results from subsequent investigations with the same variable-stability airplane (ref. 8), on the other hand, resulted in the correlation shown in figure 8(b). The latter figure shows better agreement at frequencies above 0.6 cycle per second, and, thus, tends to confirm the results from the fixed-base simulator at the higher frequencies. It is believed, therefore, that the fixed-base-simulator results are valid even at high frequencies.

Figure 9 indicates the correlation between the fixed-base and the centrifuge tests (ref. 3). Although the centrifuge tests were limited, several runs were made using closed-loop operation to check the fixed-base controllability limits for two sets of vehicle characteristics. Indicated by the fractions are the controllable, or successful, runs compared to the total number of attempted runs. These centrifuge results, although limited, are significant in that they show that large levels of static instability are controllable even under adverse acceleration environments and also under conditions of rapidly changing vehicle dynamics. The levels of static stability used to represent the configurations correspond to the most adverse condition encountered, that which occurs during staging. For a brief period the pilot is without control at these conditions. The fact that the pilot is abruptly faced with a difficult control task approaches, to some extent, the conditions of a primary stability-augmentation failure.

Lateral-Directional Control

Although two modes of motion are involved in attitude control of roll and sideslip, the modes are so interdependent that they are treated simultaneously.

In general, the controllability limits for the lateral-directional modes were similar to those of the longitudinal mode; however, because of the complexity of the lateral-directional motion, the effects of additional variables on the control task were investigated. Among these variables were effective dihedral, cross-control moments, roll damping, and control techniques. The results are discussed in terms of control technique used and the effects of the various parameters on the control task.

It should be noted in the following results that any damping (L_p, M_q, N_r) greater than the basic values given in table I resulted from the addition of ideal dampers to the basic control system. This also results in apparent changes in the rotary derivatives N_p and L_r because of the effects of cross-control terms N_{δ_a} and L_{δ_r}. Thus

$$\Delta N_p = \frac{N_{\delta_a}}{L_{\delta_a}} \Delta L_p$$

$$\Delta L_r = \frac{L_{\delta_r}}{N_{\delta_r}} \Delta N_r$$

Ailerons only.- Shown in figure 10 are the controllability limits when only ailerons are used. The area designated as A is controlled by using the ailerons in the normal manner of monitoring bank angle $(\delta_a \sim \varphi)$. This technique is used in normal (stable) flying and is also used initially by the pilot in attempting to control a dynamically unstable configuration, designated as area B. The boundaries for area A indicate that no amount of dynamic instability can be controlled with this technique, but that substantial levels of static instability are controllable (although sideslip was not monitored). The limit of the static instability that can be controlled, provided there is sufficient damping, corresponds to the condition where aileron deflection produces no roll

except for a brief transient. This condition, henceforth denoted as $\frac{dp}{d\delta_a} = 0$, exists when the rolling moment of the aileron is balanced by the rolling moment due to the sideslip created by the yawing moment of the aileron. As shown in appendix A, the parameter $\frac{dp}{d\delta_a} = 0$ when $N_\beta - \frac{L_\beta N_{\delta_a}}{L_{\delta_a}} = 0$. This segment of the controllability limit was more difficult to define than was the longitudinal controllability limit.

As the pilot gained experience in controlling a lightly damped directional mode, he also changed his control technique. By using ailerons as a yaw control $(\delta_a \sim \beta)$, the pilot was able to damp yawing oscillations and, thus, was able to control the conditions in area B. A comparison of figure 10 with figure 2 indicates that the degree of dynamic instability which pilots could control was slightly greater for the lateral-directional mode than for the longitudinal mode. With no restriction on the bank angle, the outer solid-line boundaries of areas B and C define the conditions at which the sideslip could be controlled. With the control of bank angle limited to 45°, areas B and D were controllable, but area C was not. For controlling within area D, the same technique of using ailerons to control sideslip is required, but the pilot must also purposely sideslip to create rolling moment for the control of bank angle $(\delta_a \sim \beta \sim \varphi)$. The sign of the sideslip-to-bank relationship is not determined by L_β alone, but by the sign of the $N_\beta - \frac{N_{\delta_a}}{L_{\delta_a}} L_\beta$ condition. Control in area D was, in general, quite difficult. Only after considerable briefing and practice, could pilots retain control of the aircraft. This type of control was made much easier when the $\frac{dp}{d\delta_a} = 0$ line forming the upper limit was at higher levels of stability.

The conditions corresponding to area E in figure 10, on the other hand, are easily controlled, but by a different technique. Use is made of the sideslip generated by the weight vector when the airplane is banked. The pilot, therefore, purposely banks to the left to eliminate right sideslip $(\delta_a \sim \varphi \sim \beta)$. Although the condition is below $\frac{dp}{d\delta_a} = 0$, the normal application of aileron is used. The motion is heavily damped

and presents no problem to the pilot. Because of the nature of the control, the lower limit of the area is a function of velocity, pitch angle, and angle of bank $\left(\dot{\beta} \approx \frac{g}{V} \sin \varphi \cos \theta\right)$ and is determined by the narrowing limits of sideslip which the pilot must not exceed if control is to be maintained.

Effect of N_{δ_a}: Presented in figure 11 are controllability limits for several values of yawing moment due to aileron deflection N_{δ_a}. This term has the twofold effect of (1) determining the location of the $\frac{dp}{d\delta_a} = 0$ condition, and (2) permitting the pilot to use ailerons as rudders $(\delta_a \sim \beta)$. Except for $N_{\delta_a} = 0$, the controllability limits are, essentially, identical until the directional static stability is reduced to a value at which $\frac{dp}{d\delta_a} = 0$. At this point, the controllability limit lies just above the $\frac{dp}{d\delta_a} = 0$ line $\left(\text{as shown for } N_{\delta_a} \approx B, 0, -B\right)$ until at higher values of $2\zeta\omega_n$ it is possible to use the control technique $\left(\delta_a \sim \varphi \sim \beta\right)$, thereby enabling more unstable characteristics to be controlled.

With the basic value of N_{δ_a}, appreciable dynamic instability could be controlled by using ailerons as rudders $\left(\delta_a \sim \beta\right)$. For $N_{\delta_a} = 0$ no dynamically unstable conditions could be controlled, since the ailerons produced no yawing moment. This is not true at high angles of attack of the principal axis, however, because of the sideslip produced by rolling. Many values of N_{δ_a} were investigated at $\omega_n^2 = 15.6$ to obtain a more extensive definition of the controllability limits as a function of N_{δ_a}. Figure 12 indicates the level of dynamic instability that can be controlled though N_{δ_a} increases rapidly from $N_{\delta_a} = 0$. The basic value of N_{δ_a} proved to be near optimum for this control task.

Effect of L_β: Presented in figure 13 are the changes in the controllability boundary due to variations of the dihedral effect L_β. The effect of L_β is twofold, inasmuch as both the φ/β ratio and the

location of the $\frac{dp}{d\delta_a} = 0$ line are dependent on L_β. Consequently, areas D and E, which were presented in figure 10 and discussed previously, are sensitive to this parameter. Area D was not included because of the difficulty it presented in defining the controllability boundary. At the larger values of φ/β it becomes more difficult to control φ through β and, consequently, less instability can be tolerated. This was particularly noticeable for the $L_\beta = 4B$ boundary of figure 13. The effect of φ/β ratios corresponding to smaller changes in L_β was not noticeable.

Effects of a roll damper: The effects of including an ideal roll damper were investigated for the condition in which the damping of the combined airplane-damper was $L_p = -10$. A corresponding change in N_p was made because of N_{δ_a}, as discussed at the beginning of the Lateral-Directional Control section. Figure 14 indicates that when ailerons only were used to control bank angle in the normal manner $(\delta_a \sim \varphi)$, the addition of a roll damper made control easier for low values of damping and static stability. It also enabled the pilot to control the important area of low damping and stability, but did not allow control of a dynamically unstable condition.

Ailerons and rudder.- From several standpoints, using both ailerons and rudder for control proved to be superior to using ailerons only. First, it was not necessary to learn new piloting techniques. Second, no limit such as $\frac{dp}{d\delta_a} = 0$ was found which had any significance, provided the rudder produced considerably more yawing to rolling moment than was produced by the aileron. Compared in figure 15 are controllability limits for ailerons only used normally, ailerons only with novel techniques, rudder only, and rudder used with ailerons. There was no noticeable difference in the controllability limits whether or not ailerons were used with the rudder.

Large values of L_β had an adverse effect on the controllability limit, much the same as when ailerons only were used. While roll damping generally made controlling easier, little change was evidenced in the controllability limits (see fig. 14).

Other effects.- For the conditions studied, small changes in the trim angle of attack of the principal axis α_0 had little effect on the controllability limits. The effect of large α_0 was not

investigated. It should be pointed out that although a large negative product of α_0 and effective dihedral results in a large increase in the static (stick-fixed) stability $\omega_{n_\psi}^2 \approx N_\beta - \alpha_0 L_\beta$, this effect is of no benefit to the pilot if he maintains a wings-level attitude. The latter technique, as shown in appendix A, effectively reduces the static stability (pilot-airplane) to $\omega_{n_\psi}^2 \approx N_\beta - L_\beta \frac{N_{\delta_a}}{L_{\delta_a}}$.

The effect of pilot learning, as mentioned previously, was primarily that of change in technique, as shown in figure 16. However, at conditions of considerable damping when controllability is limited by $\frac{dp}{d\delta_a} = 0$, the pilot needs little or no practice to maintain control.

Figure 17 shows the effect of a 2-second interruption of the pilot's display every 10 seconds. The results are similar to those for the longitudinal mode (fig. 5), with the exception of conditions of considerable damping where no change was caused by the interruption.

Correlation with other simulator investigations and flight tests.- To determine the correlation for varying degrees of simulation, a comparison of controllability limits defined by using the simple, nonmoving simulator is made in figure 18 with similar results from the motion simulator and flight tests.

Ailerons only: An investigation using a variable-stability F-86E airplane showed that a pilot can control significant levels of dynamic instability without rudders by using the yawing moment of the ailerons to control sideslip. For moderate values of dynamic instability, the pilot found that the motion was more easily controlled with ailerons than with rudders because of the lower control forces. The pilot did not continue to decrease the damping because the rudder servo-authority limit had been reached. He believed, however, that only small additional reduction in damping could be tolerated. In addition, the variable-stability airplane had only one-third the yawing moment due to aileron deflection that was used on the fixed-base simulator. A small segment of the simulator controllability limit for $N_{\delta_a} \approx 0.32B$ is shown in figure 18. The pilot did not feel that the motion stimulus of the airplane was important in controlling the motion in this condition.

The loss of control of the X-2 airplane on its final flight (ref. 9) was attributed to exceeding the limit determined by the condition of

$\frac{dp}{d\delta_a} = 0$. Although the airplane had a small amount of directional stability, the value of N_{δ_a} was negative and the effective dihedral was large, which resulted in a situation similar to, but not as extreme as, the $N_{\delta_a} = -B$ condition presented in figure 11. When the X-2 pilot attempted to correct for bank angle in the normal manner, the N_{δ_a} caused sideslip which produced a greater rolling moment than that produced directly by the ailerons, resulting in an effective control reversal. A high roll rate resulted, causing the airplane to go violently out of control. The rudder was locked during this portion of the flight.

Ailerons and rudders: Since little difference was found in the conditions that were controllable whether both ailerons and rudder or only rudder was used, no distinction is made in the following discussion.

A variable-stability F-86E airplane was flown at three different flight conditions to determine the correlation between controllability limits for $\left(\delta_r \sim \dot{\beta}\right)$ of the static simulation and actual flight, indicated by the circular symbols in figure 18. A fair degree of correlation is shown, even though large differences existed in the controller characteristics. The pilot considered the controllability limit conservative because of the high rudder forces. Appreciable force was applied simultaneously by the pilot to both pedals to increase response.

To retain control it was necessary for the pilot to keep the airplane motion very small. By using the horizon as a reference, he was able to control considerably less unstable conditions $\left(\omega_{n_\psi}^2 = -6\right)$ than those which could be controlled by using a sideslip indicator in the cockpit $\left(\omega_{n_\psi}^2 = -13\right)$. The pilot noted especially that at the intermediate flight condition $\left(\omega_{n_\psi}^2 = 2.5\right)$ the motion was unusual and, therefore, disconcerting.

Tests conducted at the NASA Langley Research Center and reported in reference 2 determined a controllability limit by adjusting the dynamics of a swiveling yaw chair. Good agreement exists between the yaw-chair and fixed-base-simulator results except at the low values of static stability, as shown in figure 18. Also shown in this figure is the extent of the conditions considered for the variable-stability F-86E airplane in the landing study of reference 5. The controllability limit was almost reached, although this was not the purpose of the study.

During an investigation with a KC-135 airplane at the NASA Flight Research Center, the yaw-damper inputs were intentionally reversed to determine if the resulting dynamic instability was controllable. The condition shown in figure 18 was not only controllable, but was flown during a landing approach to the start of the flare.

Coupled Longitudinal and Lateral-Directional Modes

A limited study of the effects of marginally stable longitudinal and lateral-directional modes determined the extent to which stability of both modes could be decreased and still be controllable. The results, which apply only to light (basic) damping of both modes, are presented in figure 19. Definition of this boundary was critical with respect to the amount of maneuvering required of the pilot. If the airplane motions were kept very small and the slow control application contained the motions, the pilot was able to control both modes. When the motions were sizable and two simultaneous corrections were required, control was usually lost. It is evident from figure 19 that at low damping little more than neutral longitudinal and directional static stability could be controlled simultaneously.

Another study on the control of these coupled modes is reported in reference 6, which shows the effects of damping on a pilot's ability to cope with a single-degree-of-freedom and a six-degree-of-freedom problem.

HUMAN-TRANSFER-FUNCTION STUDY

If a mathematical model existed which could represent the pilot during the task of controlling a marginally stable airplane, controllability limits could be determined analytically. In this study, several human transfer functions were used to calculate controllability limits. The results are briefly discussed in the following sections and in appendix B, in which supplementary derivations and considerations are given. For the calculated limits, the criterion for controllability was simply stability, rather than a set of limits on excursion amplitudes.

Controllability Limits Determined by Human Transfer Functions

In the search for human transfer functions it was noted that several investigators have determined such functions (ref. 10) by correlating a human operator's response during a tracking task to the variable being monitored. The systems being controlled were stable and were subjected to a random disturbance. The results of the correlation were

then approximated by a transfer function which described the human operator and which usually had the form

$$\text{Human transfer function} = \frac{K_e^{-Ts}\left(T_L s + 1\right)}{\left(T_I s + 1\right)\left(T_N s + 1\right)} \tag{1}$$

Because of the general acceptance of this type of transfer function, several controllability limits based on this form were investigated.

Longitudinal and directional control.- The coefficients in function (1) were chosen initially such that the lag in the pilot's response was minimized to the extent believed to be achievable by a human operator (see ref. 10). The following expression is obtained

$$\frac{M_{\delta_e}\delta_e(s)}{\alpha(s)} = -\frac{e^{-0.2s}(2.5s + 1)}{(0.1s + 1)^2} \tag{2}$$

The results from this function are compared in figure 20 with controllability limits derived from the simulator study and, although shown for longitudinal control, apply equally well to directional control. The poor agreement shown may indicate that the transfer function does not accurately describe the pilot performing this control task, or that the pilot's transfer function changes appreciably with changes in the characteristics of the controlled element. In spite of the poor agreement, this form was used with success in the study of handling qualities (refs. 11 and 12) of marginal configurations.

By extending the range of the coefficients used in the conventional form of the human transfer function, it is possible to approximate closely the statically stable portion of the controllability limit. This was done by using the following form of the transfer function given in reference 2

$$\frac{M_{\delta_e}\delta_e(s)}{\alpha(s)} = -1.6se^{-0.13s} \tag{3}$$

The resulting controllability limit is seen in figure 20 to be in good agreement with the simulator results in the statically stable range. The continuing trend of the lower (unstable) portion of the

controllability limit, however, cannot be duplicated by using conventional human transfer functions which have bounded amplitude ratios. As shown in appendix B, an unbounded amplitude ratio is required to stabilize the continuously increasing static instability. Otherwise, the lower portion would be flat, as illustrated in figure 20 by transfer functions (2) and (3). This would suggest that an integral term should be included in the transfer function. The integral term, however, would produce a 90° phase lag which requires not only a reduction in the phase lags produced in the other factors, but additional lead terms.

Because of the resulting complexity, a simpler form of transfer function was sought with the properties of an unbounded gain and sufficient lead. A function having the form

$$\frac{M_{\delta_e}\delta_e(s)}{\alpha(s)} = -\frac{65e^{0.45s}}{s} \qquad (4)$$

was found to approximate closely the controllability limits for angle-of-attack control, sideslip control using ailerons only, and sideslip control using rudder. The controllability limits calculated for function (4) are compared to the simulator-derived controllability limits for the longitudinal and directional control tasks in figure 21. The correlation is fairly good. Only one calculated limit is presented because the differences resulting from slightly different airplane transfer functions are minor. The poorer approximation shown at large values of airplane damping is caused by the excessive phase lag of the "pilot" at low frequencies of the pilot-airplane combination. As the frequency approaches 0, the phase angle φ of the human transfer function approaches a lag of 90°, making control of a statically unstable condition impossible. This form of the transfer function may, at first, seem rather unconventional, since perfect anticipation (indicated by the positive exponent) does not exist in practice; however, it becomes more reasonable when considered merely as a convenient approximation for the complex multiple lead network, which might better approximate the pilot's true transfer function. Nor does prediction on the part of the pilot seem unreasonable when it is considered that, after controlling the airplane for a short time without an unknown disturbing function, the pilot becomes very familiar with the control problem.

Lateral control.- By using human transfer functions, lateral controllability limits were also calculated. These limits were particularly difficult to define at low levels of damping and stability. The use of function (4) for lateral control ($\delta_a \sim \varphi$) virtually eliminated the area,

shown by the shaded portion of figure 22, at low levels of damping and static stability which was found to be uncontrollable during the simulator program. Better correlation between the calculated boundary and the experimental results was obtained by representing the pilot as a proportional-plus-derivative controller (fig. 22). By considering the pilot as a proportional controller only, a larger unstable area of vehicle damping and static stability was produced. An increase in the pilot's gain further increased the uncontrollable area. This result is in agreement with the pilots' comments that the greater effort they put into restricting the airplane motion, the more likely they were to lose control.

Development of a Composite Human Transfer Function

In this section a human transfer function is developed which matches more closely the controllability limits found in the simulator tests discussed earlier. In general, a function is desired which is defined by disturbances created solely by the pilot. Unfortunately, nothing is gained in a control task of the type under consideration simply by correlating the input and output of the pilot $\frac{\delta_e(s)}{\alpha(s)}$, since the resulting transfer function is merely the inverse of the airplane transfer function, that is

$$\frac{\alpha(s)}{\delta_e(s)} = \frac{M_{\delta_e}}{s^2 + 2\zeta\omega_n s + \omega_n^2}$$

It is possible, however, to determine, by other means, a composite transfer function which has the same gain and phase angle as the pilot at the predominant controlling frequency (that is, the frequency of the undamped oscillation at the controllability limit). No two points on the boundary may have the same controlling frequency, since the resulting human transfer function would have to be multivalued. If the pilot's transfer function does not change along the controllability limit, this composite transfer function will equal that of the pilot; if the pilot's function changes gradually, the two will be very similar, especially near the primary controlling frequency. It should be noted, however, that all transfer functions which duplicate the controllability limit will not necessarily have these properties. For example, transfer function (4) matches closely the controllability limit but has an excessive phase lead at the higher frequencies. The composite human transfer function, on the other hand, does give the correct pilot gain

and phase angle at the predominant controlling frequencies along the controllability limit and, furthermore, is unique within the accuracy with which it is determined.

It is useful to consider the difference between the actual response of the pilot and that obtained by using a human transfer function as a forcing function. Then, if at conditions just beyond the controllability limit the composite transfer function for the pilot and the airplane is dynamically unstable, it is reasonable to assume, as previously noted, that the primary controlling frequency in the immediate proximity of the controllability limit is that for neutral dynamic stability of the pilot-airplane combination. It is then possible to determine a relationship between pilot gain and phase angle at each point on the controllability limit by determining the primary controlling frequency with harmonic-analysis techniques and by making use of the following relationships developed in appendix B

$$2\zeta\omega_n = \frac{-K \sin \varphi}{\omega} \tag{5}$$

$$\omega_n^2 = \omega^2 - K \cos \varphi \tag{6}$$

where

$2\zeta\omega_n$ damping of the airplane

ω_n^2 static stability of the airplane

$K = M_{\delta_e} \frac{d\delta_e}{d\alpha}$ gain of the pilot at the frequency ω

φ phase angle of the pilot at the frequency ω

ω predominant controlling frequency

Since these relationships are derived for the condition of neutral stability, they are applicable only at the controllability limit.

The pilot's phase angle must be zero at the point on the controllability limit for $2\zeta\omega_n = 0$ (eq. (5)). Thus, it is possible to determine the gain of the pilot from equation (6) once the predominant controlling frequency is known. This frequency was found to be approximately 2 radians per second from a harmonic analysis of a typical time

history of the pilot flying a statically unstable configuration having zero damping close to the controllability limit. From the relationships of equations (5) and (6) the pilot gain $\left(K = \left|M_{\delta_e}\right|\frac{d\delta_e}{d\alpha}\right)$ was found, therefore, to be approximately 8.

It is apparent from these relationships (eqs. (5) and (6)) that the phase angle must be positive if the pilot is to be able to control dynamically unstable conditions. It is reasonable also to assume that the phase angle of the pilot returns to zero at $\omega = 10$ radians/second (see fig. 2), although it should be noted that the irregularity of the pilot's control at such high frequencies cannot be accurately represented by a transfer function. For the pilot to be able to control conditions indicated by the continuing trend of the lower portion of the controllability limit, it can be shown that the gain of the pilot must increase without bounds and the phase angle must approach its limiting value in a particular manner. If the limiting value of ω is assumed to be zero, the phase angle will approach zero at a slope $\frac{d\varphi}{d\omega}$ equal to -0.25. The development is given in detail in appendix B.

The human transfer function presented in figure 23 (short dashes) is the result of using the preceding reasoning together with the experimentally determined pilot gain. The complex nature of the function, however, precluded the determination of a closed analytical expression; hence, only the graphical representation is presented.

It is interesting to note how well simple, analytically expressed forms of human transfer functions approximate the form derived for the complete controllability limit. Figure 23 shows a comparison of the various transfer functions, and figure 24 shows the resulting controllability limits and the ranges of stability and damping for which they may be used. Two of the transfer functions were presented earlier for the calculation of the controllability limits, while the remaining one $\frac{M_{\delta_e}\,\delta_e(s)}{\alpha(s)} = -\frac{10je^{-0.35}}{s}$ was created to satisfy the aforementioned requirements at low values of ω_n^2 (see appendix B). The correlation of the analytically expressed transfer functions and their corresponding controllability limits with the composite transfer function at the controllability limit found in the simulator study serves as an indication of the range over which the various transfer functions are applicable.

CONCLUDING REMARKS

A fixed-base-simulator study was made to determine longitudinal and lateral-directional controllability limits applicable for short periods of time under ideal conditions and to study the effects of various factors on these limits. Strategic areas of the controllability limits established with the simulator were verified by means of motion simulators, variable-stability airplanes, and other flight experience.

In controlling the longitudinal short-period mode, the pilot was able to control an airplane having a time to double amplitude of as little as 1 second at moderate frequencies. With adequate damping there was no limit to the amount of airplane static instability which could be controlled by the pilot, but the time to double amplitude must exceed about 0.3 second.

When using only ailerons to control the lateral-directional modes in the normal manner, no dynamic instability could be tolerated; in fact, appreciable directional damping was required when the directional static stability was low. Where the airplane was quite unstable statically, the pilot was able to maintain control merely by keeping a wings-level attitude, provided that adequate directional damping was present and that the product of rolling moment due to aileron deflection and yawing moment due to sideslip was greater than the product of rolling moment due to sideslip and yawing moment due to aileron deflection. The latter requirement had a significant effect on the lateral-directional controllability limits when only ailerons were used for control. When the novel technique of using ailerons as yaw control was used, dynamic instability as great as that tolerable in the longitudinal mode could be controlled, provided there was sufficient yawing moment due to aileron deflection. Although dihedral effect can increase the static (stick-fixed) directional stability, it was not necessarily beneficial when roll rate was kept at zero.

Roll dampers were beneficial when using ailerons to control bank angle in the normal manner, and were essential for low values of both static stability and damping.

With both ailerons and rudder available and used in the normal manner, levels of static and dynamic instability comparable to those for control of the longitudinal mode could be controlled. Large dihedral effect had an adverse effect on the location of the controllability limits when either rudder or ailerons were used to control sideslip.

Several human transfer functions were found which define controllability limits that are in fairly good agreement with those determined

from a simulator investigation. In addition, a human transfer function was derived which also had the same gain and phase angle as the pilot at primary controlling frequencies along the experimental controllability limits. However, because of the possibility that the human transfer function would change appreciably with changes in stability and damping, it cannot be stated with complete certainty that the transfer function presented is the best possible representation of the pilot flying at a particular condition.

Flight Research Center,
National Aeronautics and Space Administration,
Edwards, Calif., January 10, 1961.

APPENDIX A

TRANSFER FUNCTIONS OF THE CONTROLLED ELEMENTS

Transfer functions of the airplane's attitude-control modes are derived in the following presentation. Transfer functions of the lateral-directional modes are derived for each of the modes both in the unrestrained and the restrained condition. In particular, transfer functions are derived for lateral control in which sideslip is kept at zero and for directional control in which rolling is kept at zero. A marked difference in the control task results if one of the modes is restrained.

Longitudinal Control

For control of angle of attack the following equations of motion are believed to be adequate

$$\dot{q} = M_q q + M_\alpha \alpha + M_{\delta_e} \delta_e$$

$$\dot{\alpha} = q + Z_\alpha \alpha$$

After applying the Laplace transformation, the equations in matrix form are

α	q	δ_e
M_α	$(M_q - s)$	M_{δ_e}
$(Z_\alpha - s)$	1	0

The transfer function for control of angle of attack is

$$\frac{\alpha(s)}{\delta_e(s)} = \frac{M_{\delta_e}}{s^2 + (-M_q - Z_\alpha)s + (M_q Z_\alpha - M_\alpha)}$$

$$= \frac{M_{\delta_e}}{s^2 + 2\zeta_\theta \omega_{n_\theta} s + \omega_{n_\theta}^2}$$

Lateral Control

Ailerons only.- The following equations of motion are considered to be adequate for the control of roll rate

$$\dot{p} = L_p p + L_\beta \beta + L_{\delta_a} \delta_a$$

$$\dot{r} = N_r r + N_\beta \beta + N_{\delta_a} \delta_a$$

$$\dot{\beta} = -r + \alpha_0 p + Y_\beta \beta$$

After applying the Laplace transformation, the equations in matrix form are

β	p	r	δ_a
L_β	$(L_p - s)$	0	L_{δ_a}
N_β	0	$(N_r - s)$	N_{δ_a}
$(Y_\beta - s)$	α_0	-1	0

The transfer function for control of roll rate is:

$$\frac{p(s)}{\delta_a(s)} = \frac{L_{\delta_a} s^2 + \left(-L_{\delta_a} N_r - L_{\delta_a} Y_\beta\right) s + N_\beta L_{\delta_a} - L_\beta N_{\delta_a} + L_{\delta_a} N_r Y_\beta}{s^3 + \left(-Y_\beta - N_r - L_p\right) s^2 + \left(N_\beta - \alpha_0 L_\beta + Y_\beta N_r + Y_\beta L_p + N_r L_p\right) s - L_p N_\beta + L_\beta N_r \alpha_0 - Y_\beta N_r L_p}$$

$$\frac{p(s)}{\delta_a(s)} = \frac{K_1 s^2 + K_2 s + K_3}{\left(s + \frac{1}{\tau_\varphi}\right)\left(s^2 + 2\zeta_\psi \omega_{n_\psi} s + \omega_{n_\psi}^2\right)}$$

When the steady-state response was equal to zero $\left(\frac{dp}{d\delta_a} = 0\right)$, the pilot was unable to control in the normal sense ($\delta_a \approx \varphi$). For control to be possible in this manner

$$N_\beta > \frac{N_{\delta_a}}{L_{\delta_a}} L_\beta - Y_\beta N_r$$

For the special condition of $\alpha_0 = 0$ and $N_{\delta_a} = 0$, the transfer function reduces to the single-degree-of-freedom case

$$\frac{p(s)}{\delta_a(s)} = \frac{L_{\delta_a}}{(s - L_p)}$$

$$= \frac{L_{\delta_a}}{s + \frac{1}{\tau_\varphi}}$$

Ailerons with rudder applied for zero sideslip.- Another important consideration is the possible use of the rudder by either the pilot or an automatic control system to maintain zero sideslip. The equations of motion for a perfect controller ($\beta = 0$) in this case would be

$$\dot{p} = L_p p + L_{\delta_a}\delta_a + L_{\delta_r}\delta_r$$

$$\dot{r} = N_r r + N_{\delta_a}\delta_a + N_{\delta_r}\delta_r$$

$$0 = -r + \alpha_0 p$$

After applying the Laplace transformation, the equations in matrix form are

p	r	δ_a	δ_r
$(L_p - s)$	0	L_{δ_a}	L_{δ_r}
0	$(N_r - s)$	N_{δ_a}	N_{δ_r}
α_0	-1	0	0

The transfer function for roll control becomes

$$\frac{p(s)}{\delta_a(s)} = \frac{L_{\delta_a}N_{\delta_r} - N_{\delta_a}L_{\delta_r}}{\left(N_{\delta_r} - \alpha_0 L_{\delta_r}\right)s - \left(L_p N_{\delta_r} - \alpha_0 L_{\delta_r} N_r\right)}$$

Control is impossible when the numerator is zero, so that the following condition must exist for normal use of controls

$$L_{\delta_a} > N_{\delta_a} \frac{L_{\delta_r}}{N_{\delta_r}}$$

Directional Control

Rudder only.- The following equations of motion are used for considerations of directional control by means of the rudder alone

$$\dot{p} = L_\beta \beta + L_p p + L_{\delta_r} \delta_r$$

$$\dot{r} = N_\beta \beta + N_r r + N_{\delta_r} \delta_r$$

$$\dot{\beta} = -r + \alpha_0 p + Y_\beta \beta$$

The equations in the Laplace and matrix notation become

β	p	r	δ_r
L_β	$(L_p - s)$	0	L_{δ_r}
N_β	0	$(N_r - s)$	N_{δ_r}
$(Y_\beta - s)$	α_0	-1	0

and the transfer function for control of sideslip is

$$\frac{\beta(s)}{\delta_r(s)} = \frac{\left(-N_{\delta_r} + \alpha_0 L_{\delta_r}\right)s + \left(N_{\delta_r} L_p - \alpha_0 L_{\delta_r} N_r\right)}{s^3 + \left(-Y_\beta - N_r - L_p\right)s^2 + \left(N_\beta - \alpha_0 L_\beta + Y_\beta N_r + Y_\beta L_p + N_r L_p\right)s - L_p N_\beta + L_\beta N_r \alpha_0 - Y_\beta N_r L_p}$$

$$\frac{\beta(s)}{\delta_r(s)} = \frac{K_4 s + K_5}{\left(s + \frac{1}{T_\varphi}\right)\left(s^2 + 2\zeta_\psi \omega_{n_\psi} s + \omega_{n_\psi}^2\right)}$$

For $\alpha_0 = 0$ the transfer function simplifies to

$$\frac{\beta(s)}{\delta_r(s)} = \frac{-N_{\delta_r}}{s^2 + 2\zeta_\psi \omega_{n_\psi} s + \omega_{n_\psi}^2}$$

where

$$\omega_{n_\psi}^2 = N_\beta + N_r Y_\beta$$

$$2\zeta_\psi \omega_{n_\psi} = -N_r - Y_\beta$$

When α_0 does not equal zero, the static stability $\omega_{n_\psi}^2$ and damping $2\zeta\omega_n$ can differ appreciably from the values given in the two preceding equations, but cannot be expressed explicitly. A good approximation to $\omega_{n_\psi}^2$ can be obtained, however, for conditions in which

$$\left|N_\beta\right|, \left|\alpha_0 L_\beta\right| \gg Y_\beta, N_r, L_p$$

If the smaller terms are neglected, the characteristic equation becomes

$$s^3 + \left(N_\beta - \alpha_0 L_\beta\right)s = 0$$

and the equation for $\omega_{n_\psi}^2$ then reduces to

$$\omega_{n_\psi}^2 = N_\beta - \alpha_0 L_\beta$$

This expression is the basis for the term $C_{n_{\beta_{dynamic}}}$ given in reference 13.

Rudder with ailerons used to keep roll rate at zero.- When bank angle is closely monitored by either the pilot or an automatic system ($\varphi = 0$), a different transfer function exists

$$0 = L_\beta \beta + L_{\delta_a}\delta_a + L_{\delta_r}\delta_r$$

$$\dot{r} = N_\beta \beta + N_r r + N_{\delta_a}\delta_a + N_{\delta_r}\delta_r$$

$$\dot{\beta} = -r + Y_\beta \beta$$

which leads to the matrix

β	r	δ_a	δ_r
L_β	0	L_{δ_a}	L_{δ_r}
N_β	$(N_r - s)$	N_{δ_a}	N_{δ_r}
$(Y_\beta - s)$	-1	0	0

and the transfer function

$$\frac{\beta(s)}{\delta_r(s)} = \frac{-N_{\delta_r}L_{\delta_a} + N_{\delta_a}L_{\delta_r}}{s^2 L_{\delta_a} + \left(-L_{\delta_a}N_r - L_{\delta_a}Y_\beta\right)s + N_\beta L_{\delta_a} - L_\beta N_{\delta_a} + L_{\delta_a}Y_\beta N_r}$$

Note that, again, control is impossible in the normal manner if the numerator equals zero. Therefore

$$N_{\delta_r} > L_{\delta_r}\frac{N_{\delta_a}}{L_{\delta_a}} \quad \text{or} \quad L_{\delta_a} > N_{\delta_a}\frac{L_{\delta_r}}{N_{\delta_r}}$$

The latter condition is the same requirement as for control of bank when sideslip was kept at zero.

It is important to note that static stability $\omega_{n_\phi}^2$ is given by $N_\beta - L_\beta \frac{N_{\delta_a}}{L_{\delta_a}} + Y_\beta N_r$ which must be positive for roll control in the normal manner (without rudder). Even more important is the fact that, although large products of $\alpha_0 L_\beta$, as shown earlier, can create positive stick-fixed directional stability, the product has no effect when bank angle is closely controlled.

APPENDIX B

ADDITIONAL CONSIDERATIONS PERTINENT TO HUMAN TRANSFER FUNCTIONS

Given a human transfer function which adequately represents a pilot's capability of controlling a marginally controllable condition, it should be possible to predict whether or not a specific case is controllable. The following relationships were used in the derivation of transfer functions which may be applied in this manner but which are also compatible with the controllability limits found experimentally.

Calculation of Controllability Limits

The following development pertains to longitudinal control but is also suitable for directional control when $\alpha_0 = N_p = 0$. Consider the following loop containing both the pilot $G(s)$ and airplane $F(s)$ transfer functions.

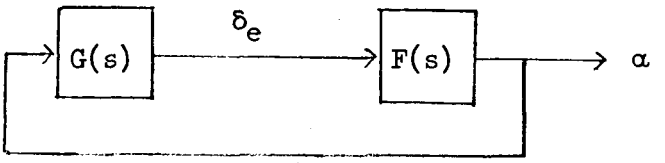

The characteristic equation for this example is

$$1 + G(s)F(s) = 0$$

Substitution of the longitudinal transfer function for the airplane (developed in appendix A)

$$F(s) = \frac{M_{\delta_e}}{s^2 + 2\zeta_\theta \omega_{n_\theta} s + \omega_{n_\theta}^2}$$

results in the equation

$$s^2 + 2\zeta_\theta \omega_{n_\theta} s + \omega_{n_\theta}^2 + M_{\delta_e} G(s) = 0$$

If only neutrally stable conditions are considered, then $s = j\omega$ where ω for the case of an undamped oscillation occurring at the controllability limit is the frequency of the controlled airplane. If the system is on the verge of becoming statically unstable, ω will equal zero.

Substituting $s = j\omega$ and equating the real and imaginary terms leads to the following two relationships

$$\omega_{n_\theta}^2 - \omega^2 + (\text{Real part})M_{\delta_e}G(j\omega) = 0$$

$$\omega 2\zeta_\theta \omega_{n_\theta} + (\text{Imaginary part})M_{\delta_e}G(j\omega) = 0$$

It is both convenient and realistic to include M_{δ_e} in the human transfer function because the pilot, in general, tries to keep the product of his gain and M_{δ_e} constant. Letting

$$K = M_{\delta_e}G(j\omega)$$

$$\varphi = \tan^{-1}\frac{(\text{Imaginary part})}{(\text{Real part})}$$

it follows that

$$2\zeta\omega_n = \frac{-K \sin\varphi}{\omega} \qquad \text{(B1)}$$

$$\omega_n^2 = \omega^2 - K\cos\varphi \qquad \text{(B2)}$$

The subscript was dropped since the result is also applicable to directional control $(\alpha_0 = N_p = 0)$. The latter two equations are used in the text of this paper and also later in this appendix for further development of the characteristics of human transfer functions.

Some Essential Characteristics of Human Transfer Functions

The two relationships (eqs. (B1) and (B2)) developed in the preceding section, together with the results shown in figure 4, enable the derivation of several essential characteristics of the human transfer function relative to its consistency with the controllability limits found in the simulator study.

First, it is evident from figure 4 that at very high controlling frequencies ($\omega \approx 10$) no amount of dynamic instability can be controlled. This condition also implies that $\varphi = 0 \pm n(180)$. The most plausible

value is believed to be $\varphi = 0$, although a transfer function is not a particularly good representation of the pilot because of the spasmodic inputs at these frequencies. For controlling conditions having negative damping, it is generally agreed that $0 < \varphi < 180^\circ$, which satisfies equation (B1). For $2\zeta\omega_n = 0$ and $\omega_n^2 < 0$, the most plausible value is again $\varphi = 0$, whereas equation (B1) indicates that $\varphi < 0$ when $\omega_n^2 < 0$ and $2\zeta\omega_n > 0$.

In addition to these generally accepted observations, it is interesting to consider what is required of the human transfer function if it is to reproduce the continuous trend of the lower portion $(\omega_n^2 \ll 0)$ of the controllability limit. Thus, solving for K from the equation (B2)

$$K = \frac{\omega^2 - \omega_n^2}{\cos \varphi}$$

and noting that $\omega^2 > 0$ and $0 < \cos \varphi < 1$, it is seen that, for the system to be stable, $K > -\omega_n^2$. If, then, there is no limit to the amount of static instability $-\omega_n^2$ controllable by the pilot, K would have to be unbounded. This quality of unboundedness is not contained in the conventional forms of human transfer functions. It is generally believed, however, that the pilot tends to keep constant the product of his gain and that of the airplane, thus enabling the use of a conventional form of human transfer function. This would cause the pilot's gain to increase as the configuration became more unstable (statically). Since the airplane transfer function

$$\frac{\alpha(s)}{\delta_e(s)} = \frac{M_{\delta_e}/\omega_n^2}{\frac{s^2}{\omega_n^2} + \frac{2\zeta}{\omega_n} s + 1}$$

has a gain inversely proportional to ω_n^2, the increase in pilot gain must be proportional to ω_n^2. The method of handling the condition of $\omega_n^2 = 0$ remains questionable, however, since the pilot gain does not go to zero.

An integral term in the human transfer function would give an ever-increasing gain as $\omega \to 0$, but would also require the phase angle to be -90° and $\omega = 0$. The latter condition is ruled out, however, when consideration is given to the ratio of damping to static stability, that is

$$\frac{2\zeta\omega_n}{\omega_n^2} = \frac{\frac{-K \sin \varphi}{\omega}}{\omega^2 - K \cos \varphi}$$

The limit of this ratio which as $\omega \to 0$ and $\varphi \to -90^\circ$ is

$$\lim_{\omega \to 0}\left(\frac{2\zeta\omega_n}{\omega_n^2}\right) = \lim_{\omega \to 0}\left(\frac{\tan \varphi}{\omega}\right) = -\infty$$

This limit implies that, contrary to actual experience, no amount of static instability $-\omega_n^2$ would be controllable at very large levels of damping. This reasoning explains why the controllability limit calculated using $\frac{M_{\delta_e}\delta_e(s)}{\alpha(s)} = \frac{-65e^{0.45s}}{s}$ does not follow the controllability limit found experimentally at conditions of high static instability $-\omega_n^2$. Experimentally determined controllability limits for $\frac{2\zeta\omega_n}{\omega_n^2}$, on the other hand, indicate a limiting value of -0.25. This, in turn, requires that $\varphi = 0$ at $\omega = 0$ and $\frac{d\varphi}{d\omega} = -0.25$. A relatively simple transfer function which will satisfy these requirements at $\omega = 0$ is

$$\frac{M_{\delta_e}\delta_e(s)}{\alpha(s)} = -\frac{K_1 j e^{-0.25s}}{s}$$

The term $j = \left(\sqrt{-1}\right)$ is introduced in order that $\varphi = 0$ at $\omega = 0$. Figure 24 shows that this type of transfer function is a good representation of the lower portion of the controllability limit.

REFERENCES

1. Harper, Robert P., Jr.: Flight Evaluations of Various Longitudinal Handling Qualities in a Variable-Stability Jet Fighter. WADC Tech. Rep. 55-299 (Contract No. AF 33(038)-20659), Wright Air Dev. Center, U.S. Air Force, July 1955.

2. Cheatham, Donald C.: A Study of the Characteristics of Human-Pilot Control Response to Simulated Aircraft Lateral Motions. NACA Rep. 1197, 1954. (Supersedes NACA RM L52C17.)

3. Holleman, Euclid C., Armstrong, Neil A., and Andrews, William H.: Utilization of the Pilot in the Launch and Injection of a Multistage Orbital Vehicle. Paper No. 60-16, Inst. Aero. Sci., Jan. 1960.

4. McFadden, Norman M., Pauli, Frank A., and Heinle, Donovan R.: A Flight Study of Longitudinal-Control-System Dynamic Characteristics by the Use of a Variable-Control-System Airplane. NACA RM A57L10, 1958.

5. McNeill, Walter E., and Vomaske, Richard F.: A Flight Investigation to Determine the Lateral Oscillatory Damping Acceptable for an Airplane in the Landing Approach. NASA MEMO 12-10-58A, 1959.

6. Creer, Brent Y., Heinle, Donovan R., and Wingrove, Rodney C.: Study of Stability and Control Characteristics of Atmosphere-Entry Type Aircraft Through Use of Piloted Flight Simulators. Paper No. 59-129, Inst. Aero. Sci., Oct. 1959.

7. Rathert, George A., Jr., Creer, Brent Y., and Douvillier, Joseph G., Jr.: Use of Flight Simulators for Pilot-Control Problems. NASA MEMO 3-6-59A, 1959.

8. Chalk, Charles R.: Additional Flight Evaluations of Various Longitudinal Handling Qualities in a Variable-Stability Jet Fighter. Part II. WADC Tech. Rep. 57-719 (Contract No. AF 33(616)-3990), Wright Air Dev. Center, U.S. Air Force, July 1958.

9. Day, Richard E., and Reisert, Donald: Flight Behavior of the X-2 Research Airplane to a Mach Number of 3.20 and a Geometric Altitude of 126,200 Feet. NASA TM X-137, 1959.

10. Anon.: Application of Human Response Data to Aircraft Design. Memo Rep. No. 69 (Contract No. AF 33(616)-3080), Control Specialists, Inc., June 7, 1956.

11. McRuer, Duane T., Ashkenas, Irving L., and Guerre, Charles L.: A Systems Analysis View of Longitudinal Flying Qualities. WADC Tech. Rep. 60-43 (Contract No. AF 33(616)-5661), Wright Air Dev. Center, U.S. Air Force, Jan. 1960.

12. Ashkenas, Irving L., and McRuer, Duane T.: The Determination of Lateral Handling Quality Requirements From Airframe-Human Pilot System Studies. WADC Tech. Rep. 59-135 (Contract No. AF 33(616)-5661), Wright Air Dev. Center, U.S. Air Force, June 1959. (Available from ASTIA as AD 212 152.)

13. Moul, Martin T., and Paulson, John W.: Dynamic Lateral Behavior of High-Performance Aircraft. NACA RM L58E16, 1958.

TABLE I.- BASIC SET OF CHARACTERISTICS OF THE GENERALIZED MACH 3 AIRPLANE USED IN THE ANALOG SIMULATOR STUDY

$\frac{I_Y - I_Z}{I_X} = -0.70$	$M_q = -0.66$
$\frac{I_{X_e} p_e}{I_Y} = 0.11$	$M_\alpha = -43$
$\frac{I_Z - I_X}{I_Y} = 0.97$	$M_{\delta_e}\left\|\delta_{e_{max}}\right\| = -2.7$
$\frac{I_{X_e} p_e}{I_Z} = 0.10$	$N_p = 0.038$
$\frac{I_X - I_Y}{I_Z} = -0.84$	$N_r = -0.14$
$L_p = -1.74$	$N_\beta = 15.6$
$L_r = 0.51$	$N_{\delta_a}\left\|\delta_{a_{max}}\right\| = 0.94$
$L_\beta = -85$	$N_{\delta_r}\left\|\delta_{r_{max}}\right\| = -2.3$
$L_{\delta_a}\left\|\delta_{a_{max}}\right\| = 10.3$	$Y_\beta = -0.23$
$L_{\delta_r}\left\|\delta_{r_{max}}\right\| = 6.3$	$Z_\alpha = -0.52$

TABLE II.- LATERAL-DIRECTIONAL DERIVATIVES USED IN THE VARIABLE-STABILITY-AIRPLANE PROGRAM

Derivative	Static stability $\left(\omega_{n_\downarrow}^2 < 0\right)$	Damping $(2\zeta\omega n < 0)$
L_β	-27.5	-42.9
L_p	-3.4	-4.6
L_r	0.9	1.0
$L_{\delta_a}\lvert\delta_{a_{max}}\rvert$	6.8	8.7
$L_{\delta_r}\lvert\delta_{r_{max}}\rvert$	0.5	1.1
N_β	(Varied)	19.0, 2.5
N_p	-0.1	-0.1
N_r	-4.0	(Varied)
$N_{\delta_a}\lvert\delta_{a_{max}}\rvert$	0.1	0.3
$N_{\delta_r}\lvert\delta_{r_{max}}\rvert$	-0.9	-1.4

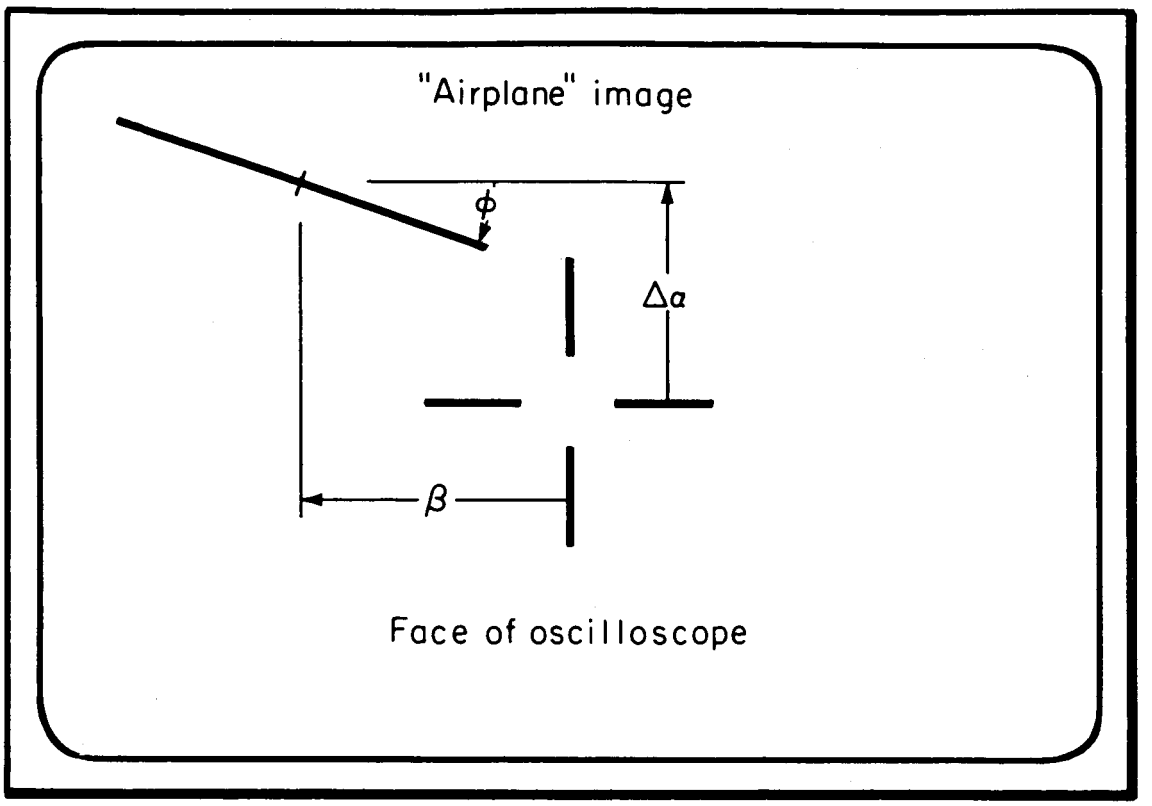

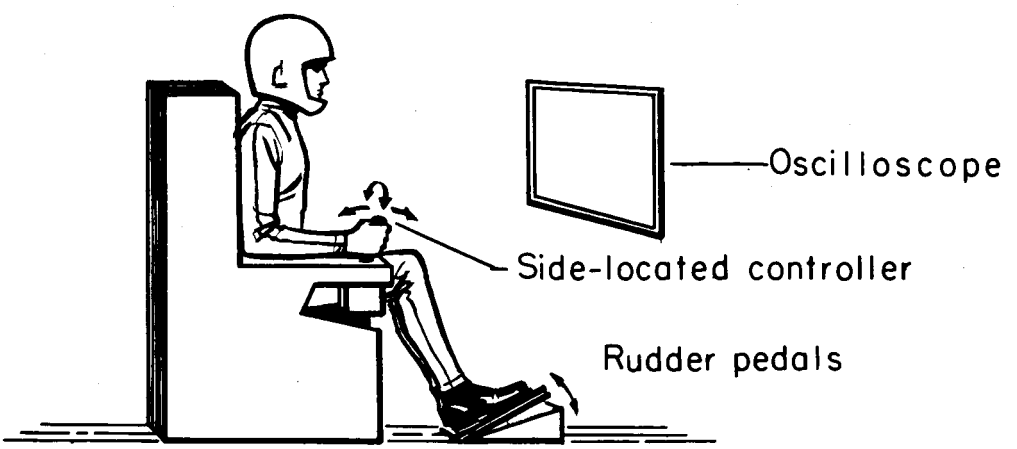

Figure 1.- Fixed-base flight-simulator arrangement.

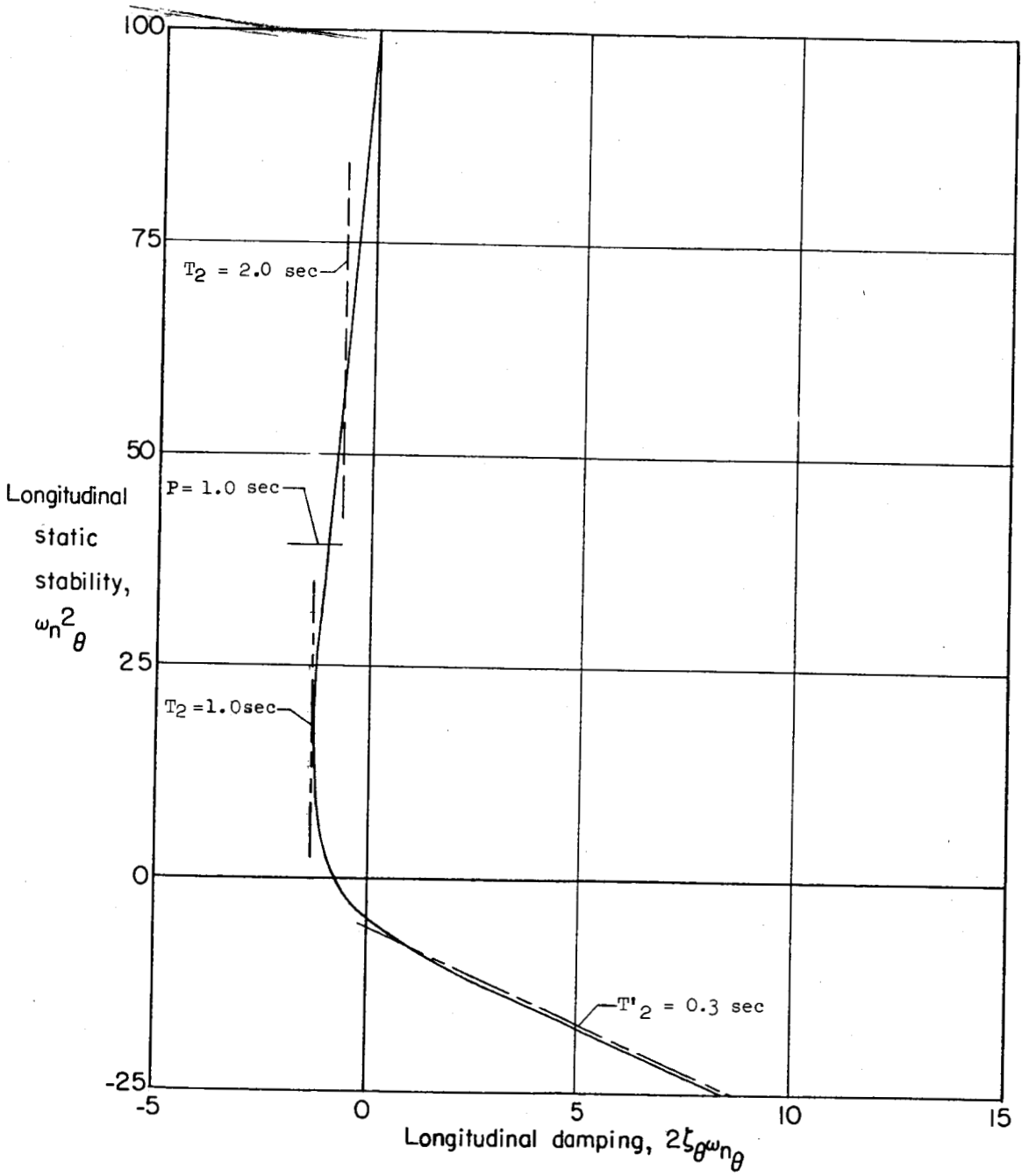

Figure 2.- Longitudinal controllability limit.

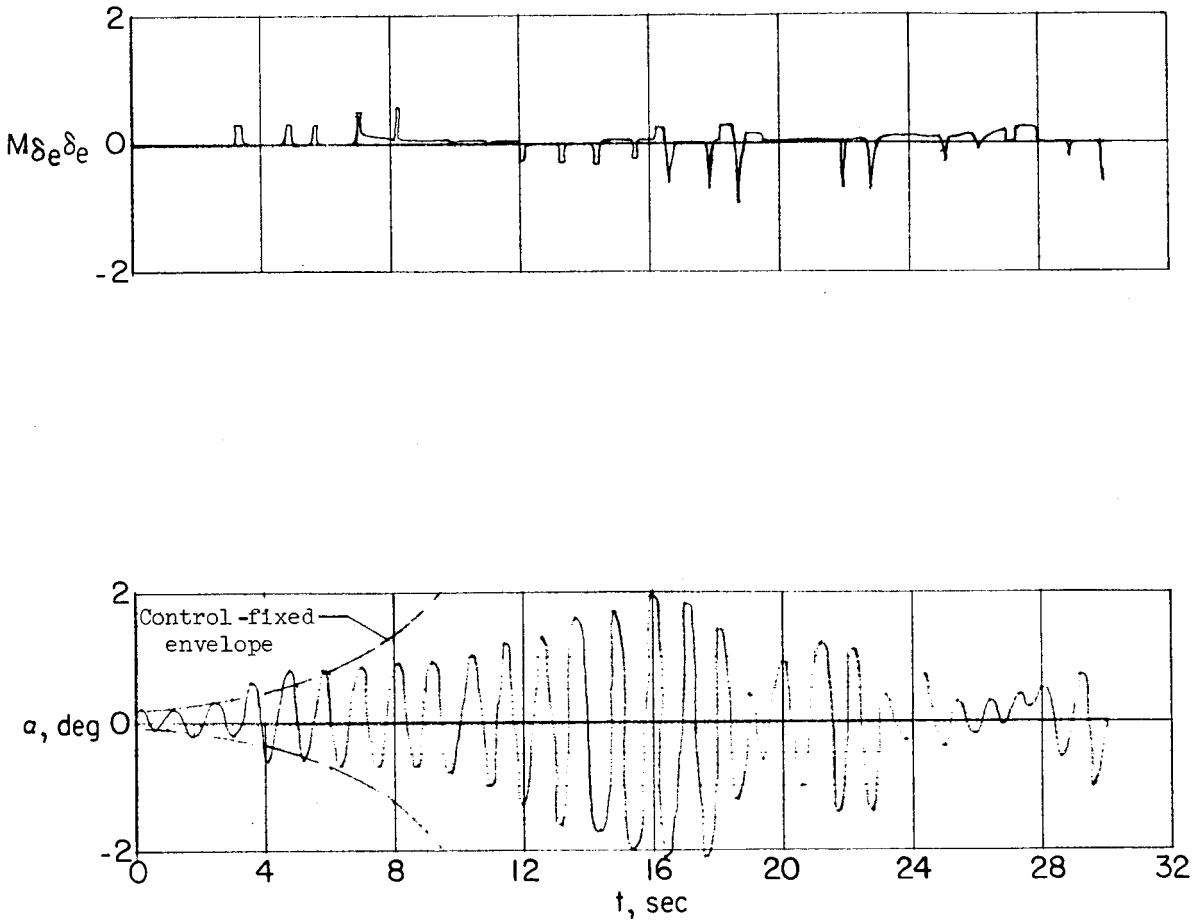

(a) High-frequency condition. $\omega_{n_\theta}^2 = 35$; $2\zeta\omega_{n_\theta} = -0.6$.

Figure 3.- Piloting characteristics at various conditions.

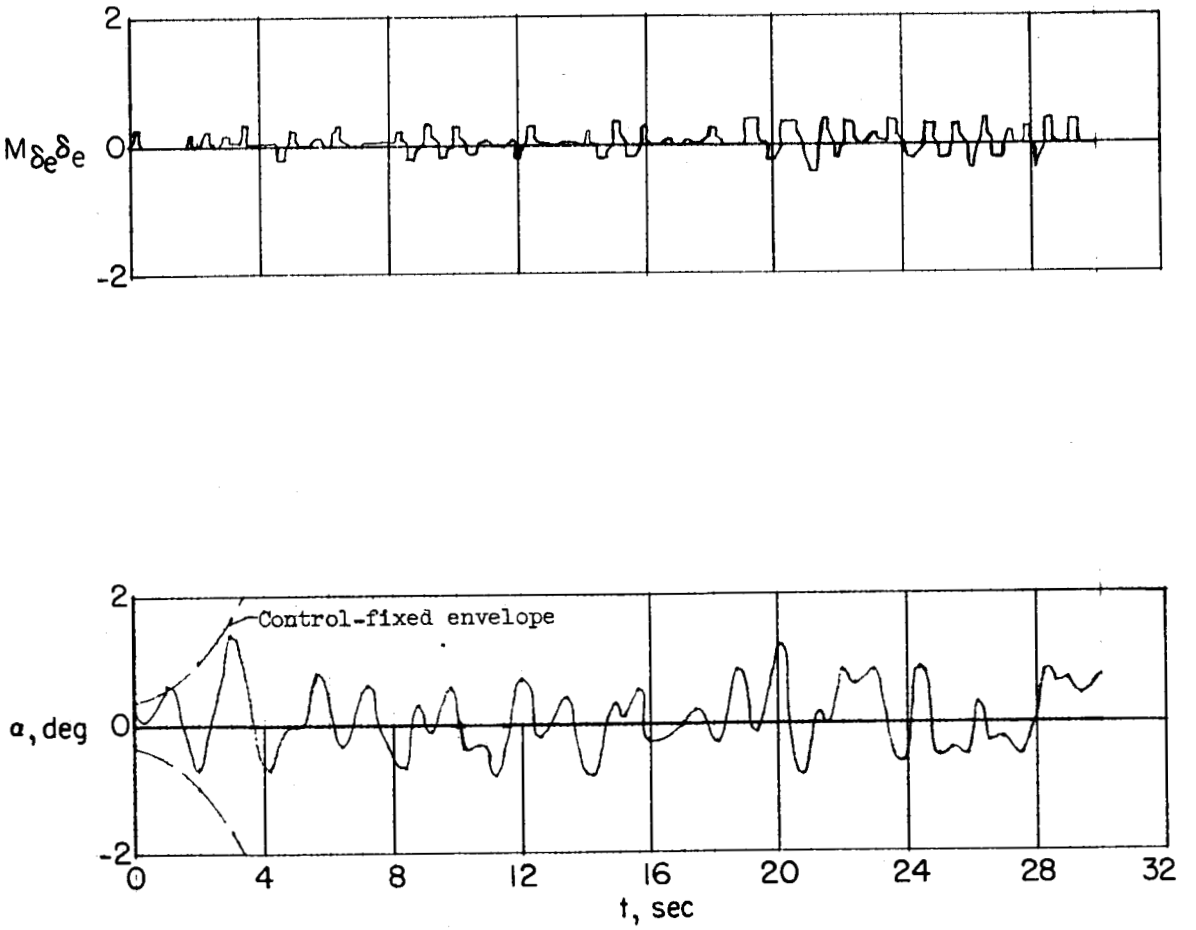

(b) Low-frequency condition. $\omega_{n_\theta}^2 = 9$; $2\zeta\omega_{n_\theta} = -1.0$.

Figure 3.- Continued.

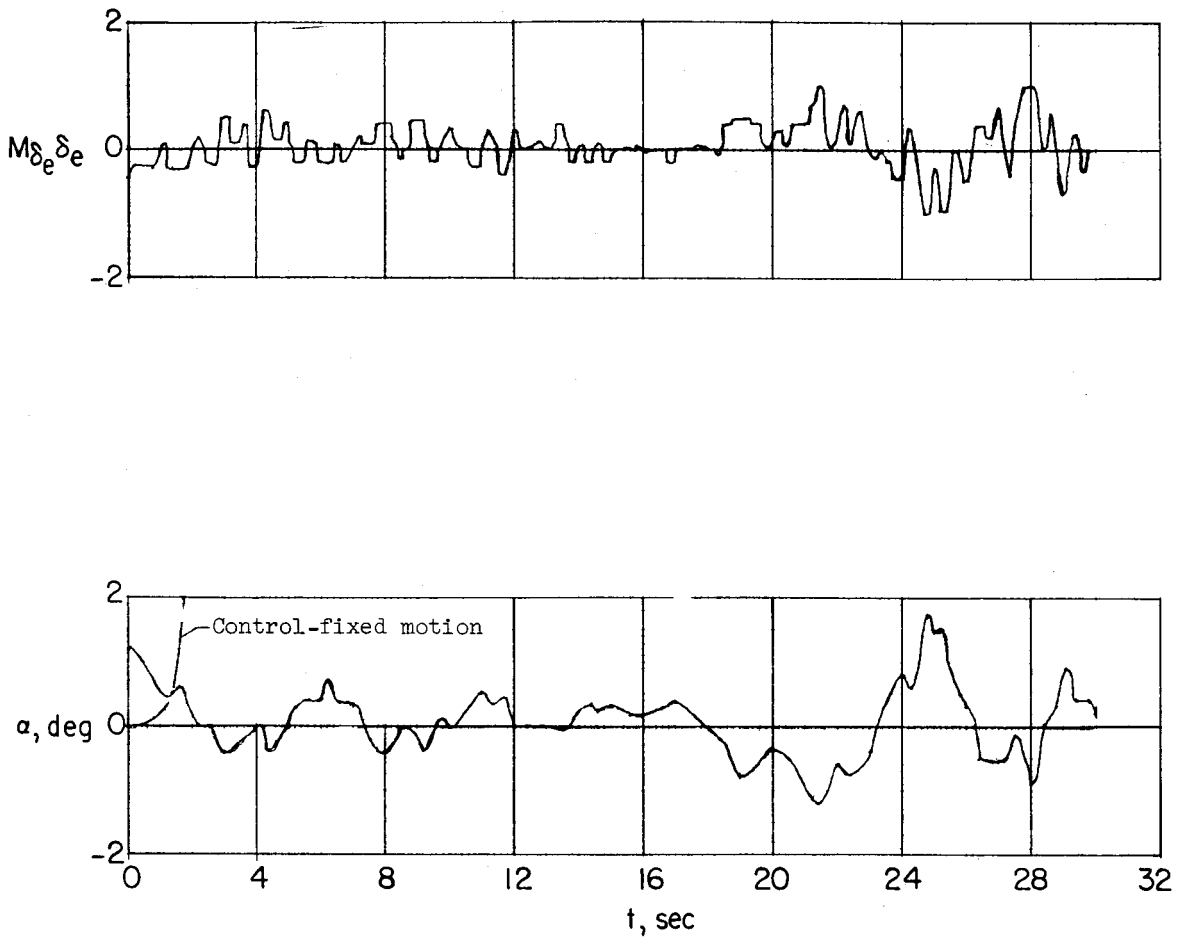

(c) Purely divergent condition. $\omega_{n_\theta}^2 = -17$; $2\zeta\omega_{n_\theta} = 6.5$.

Figure 3.- Concluded.

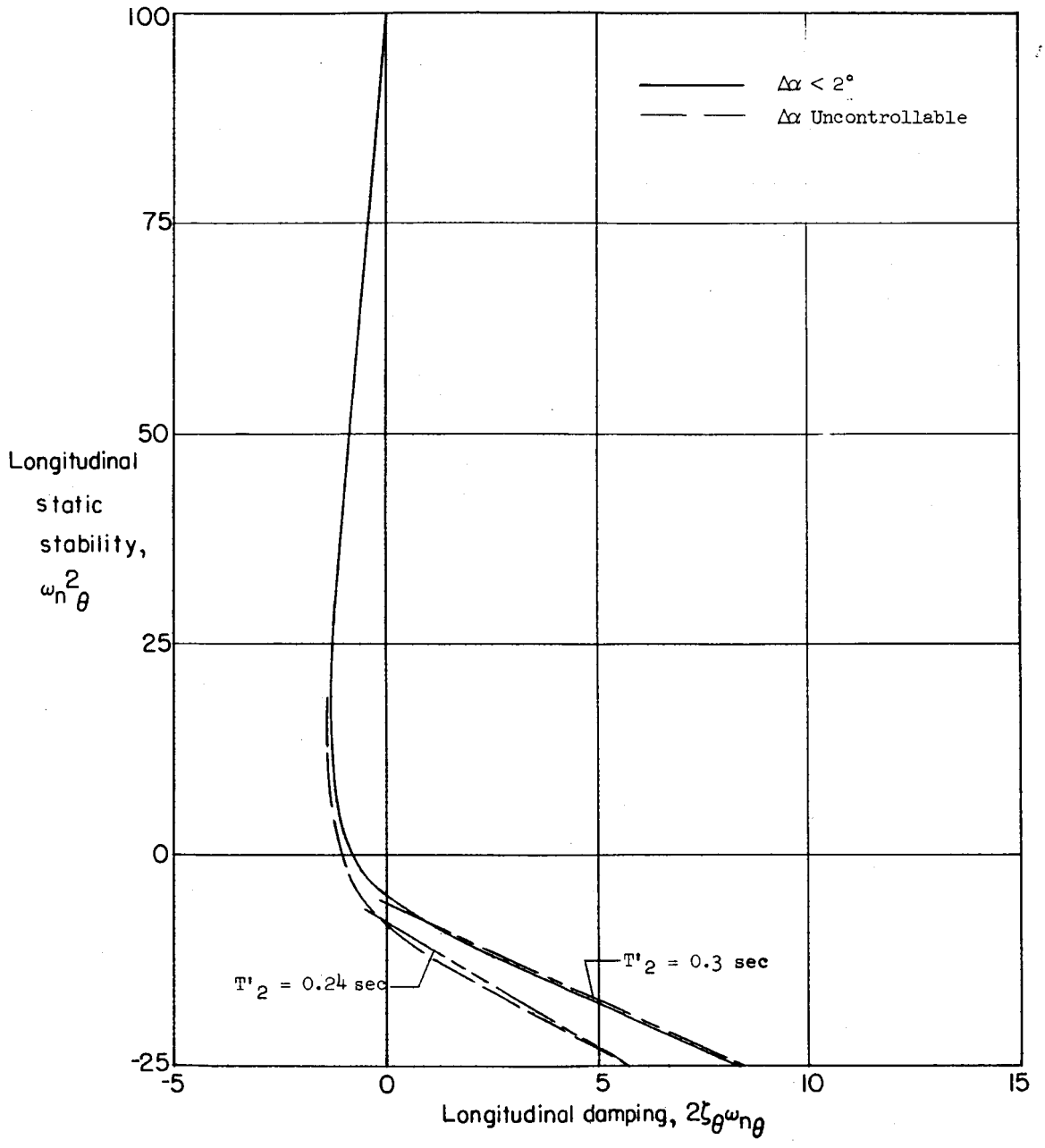

Figure 4.- Effect of controllability criteria on longitudinal controllability limit.

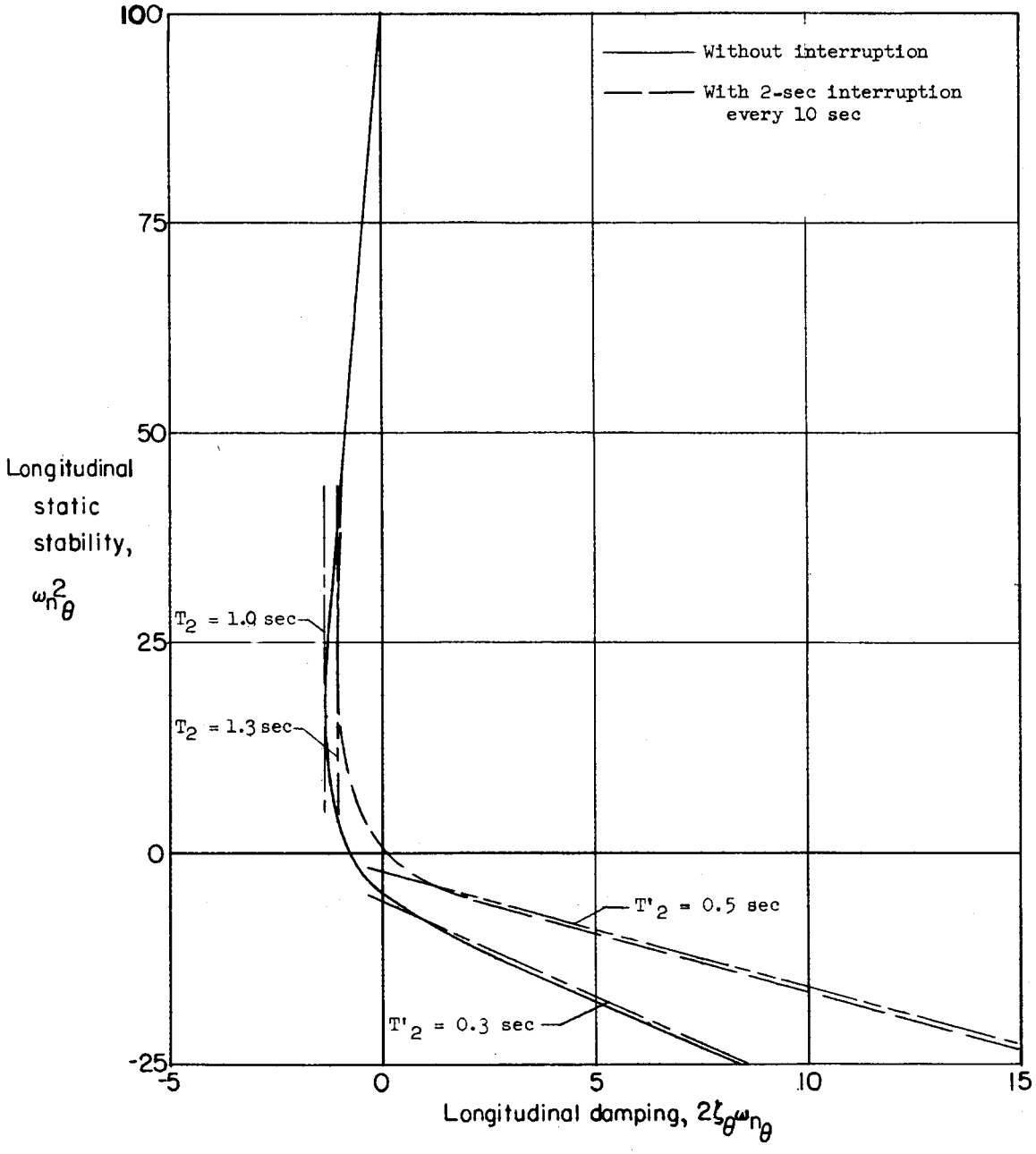

Figure 5.- Effect of a periodic 2-second interruption in pilot's presentation.

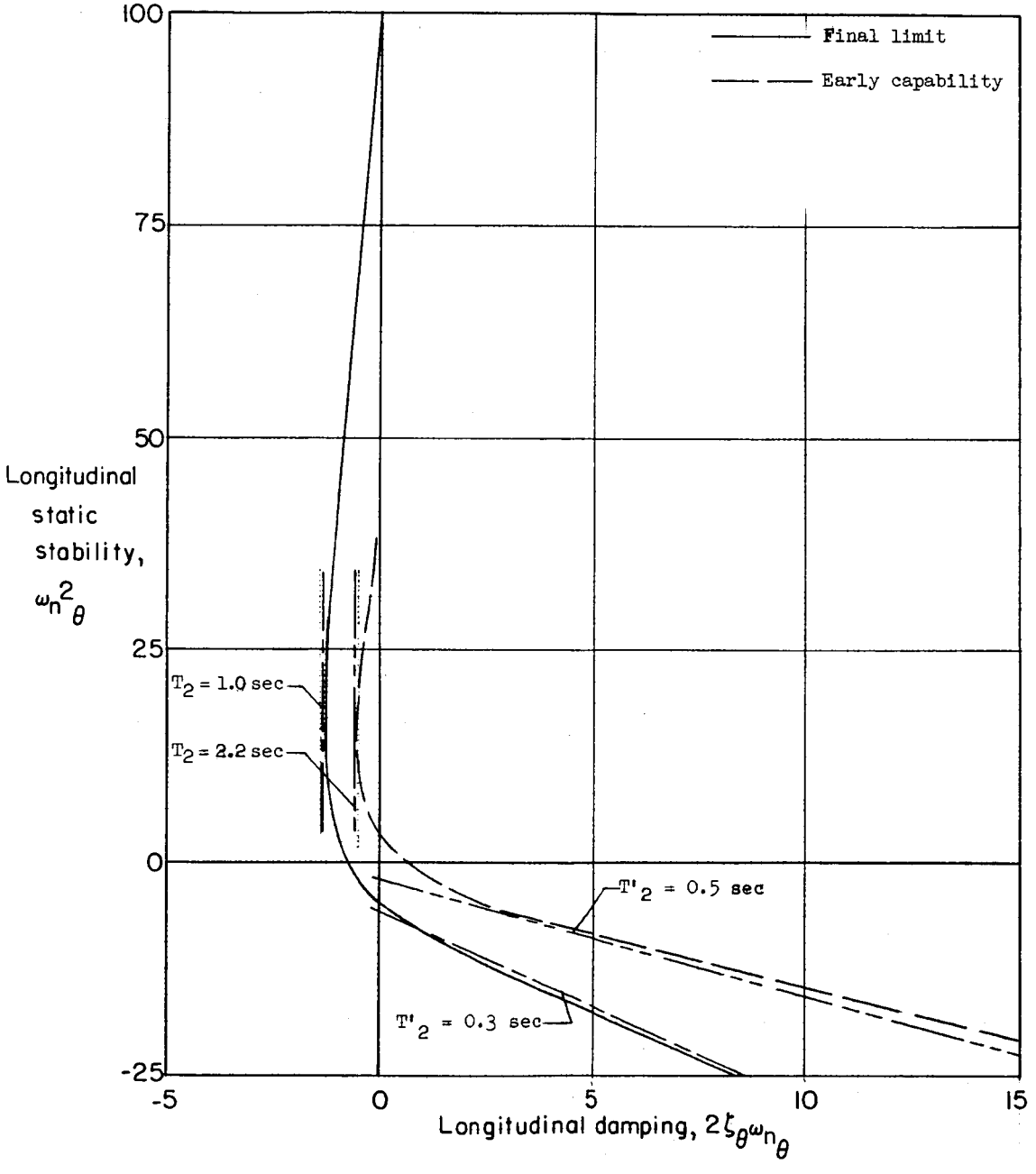

Figure 6.- Effect of pilot learning on the longitudinal controllability limit.

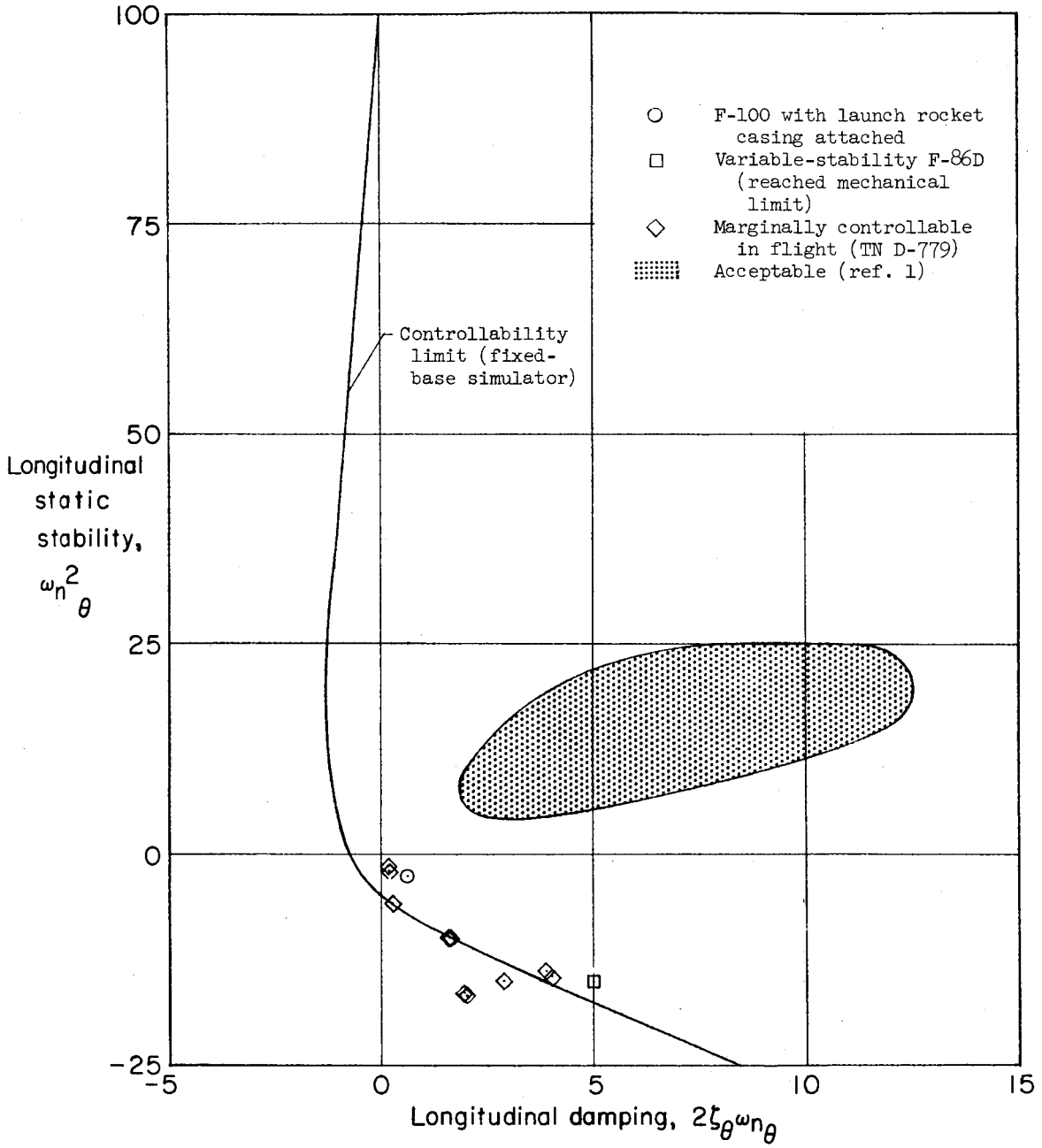

Figure 7.- Verification of longitudinal controllability limit with flight tests.

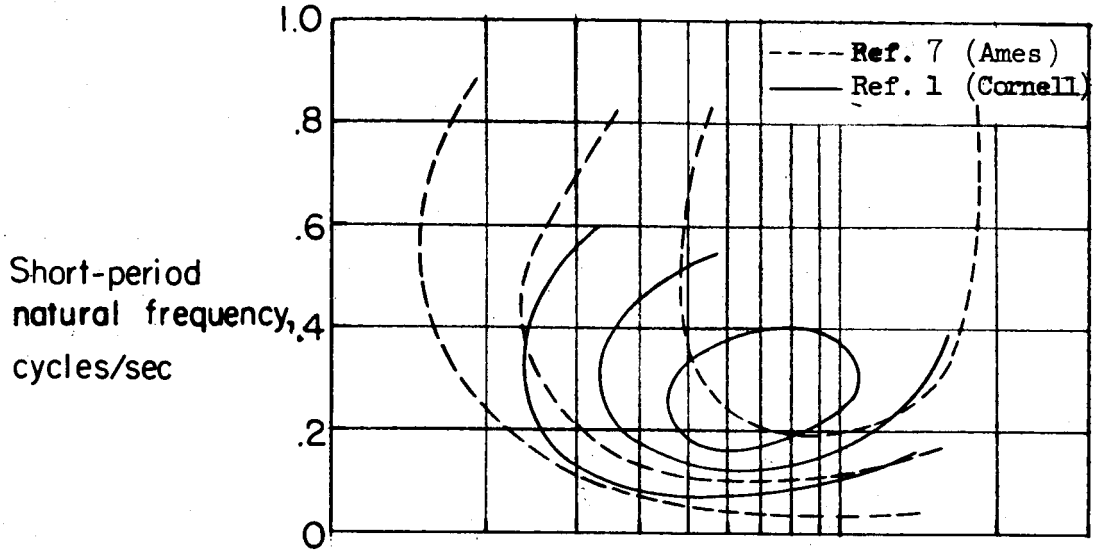

(a) Early Cornell flight tests and Ames fixed-base simulation.

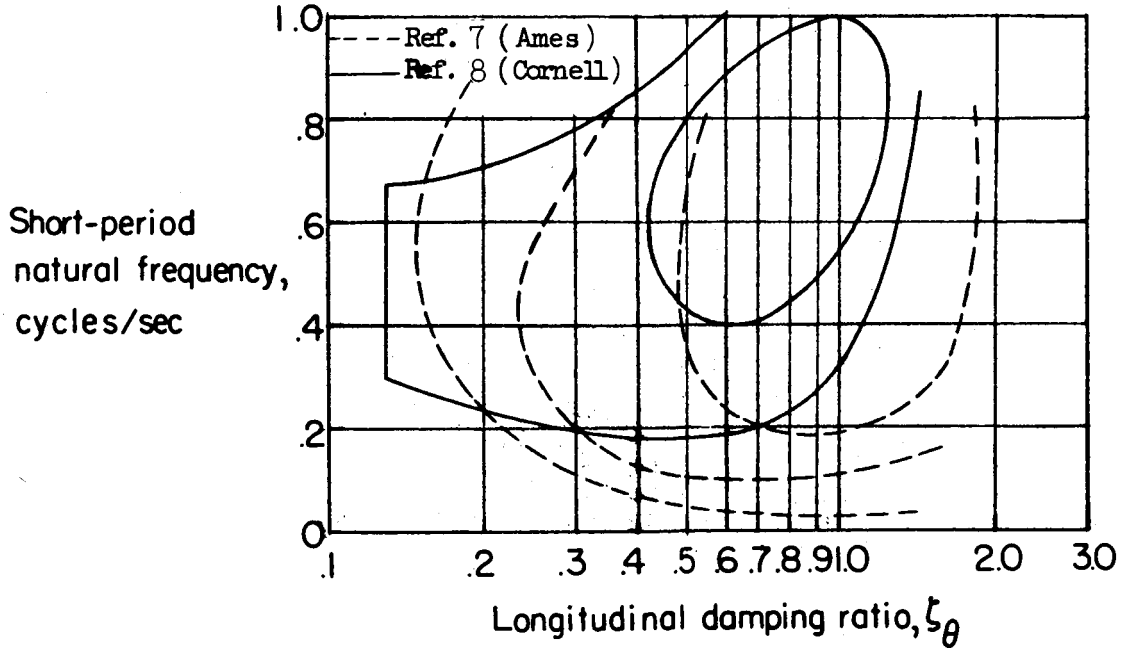

(b) Subsequent Cornell flight tests and Ames fixed-base simulation.

Figure 8.- Correlation of lines of constant pilot opinion determined from flight tests and fixed-base-simulator tests.

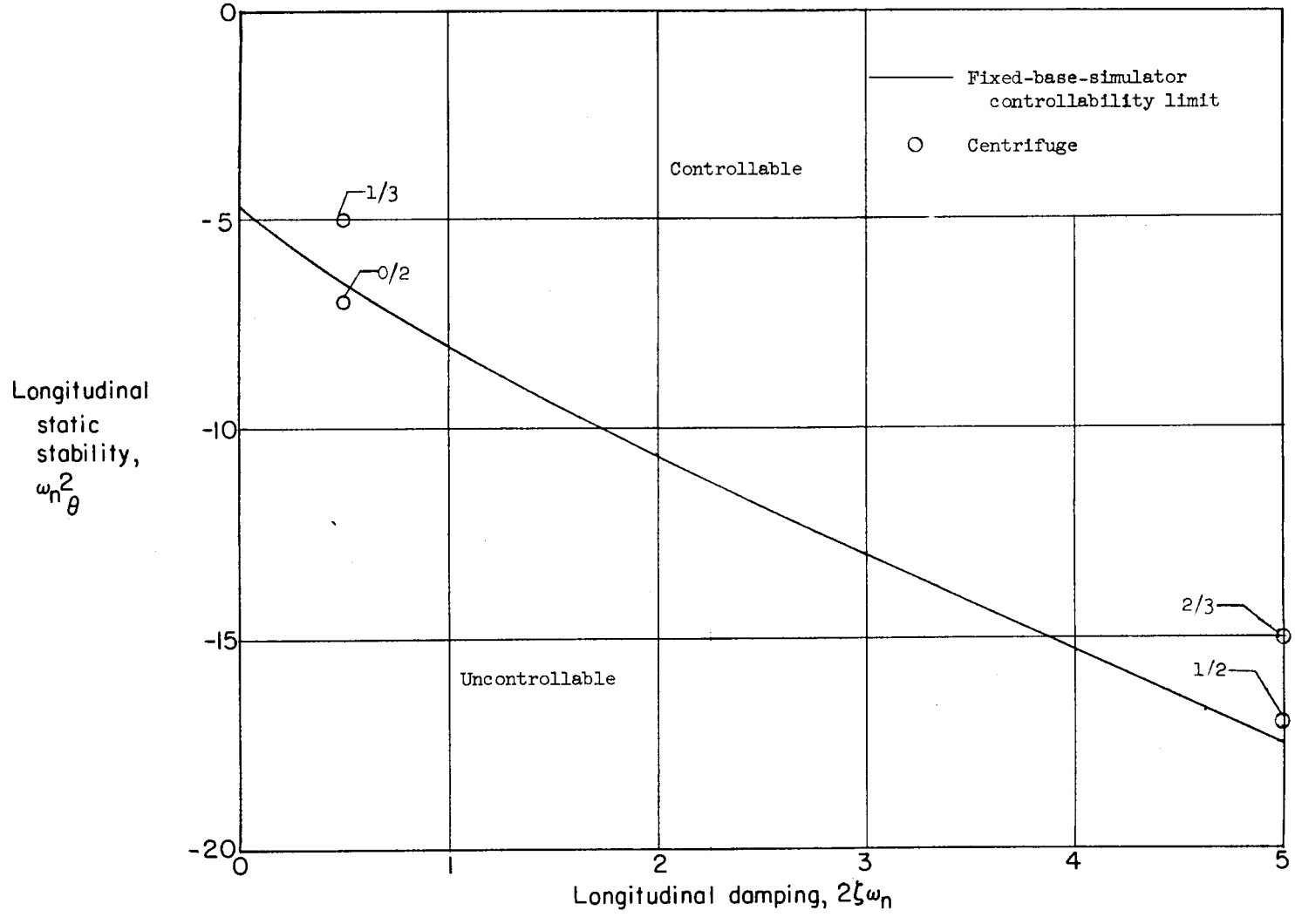

Figure 9.- Comparison of centrifuge test results with the longitudinal-controllability limit. Fractions indicate ratio of the number of successful runs to the number of attempted runs.

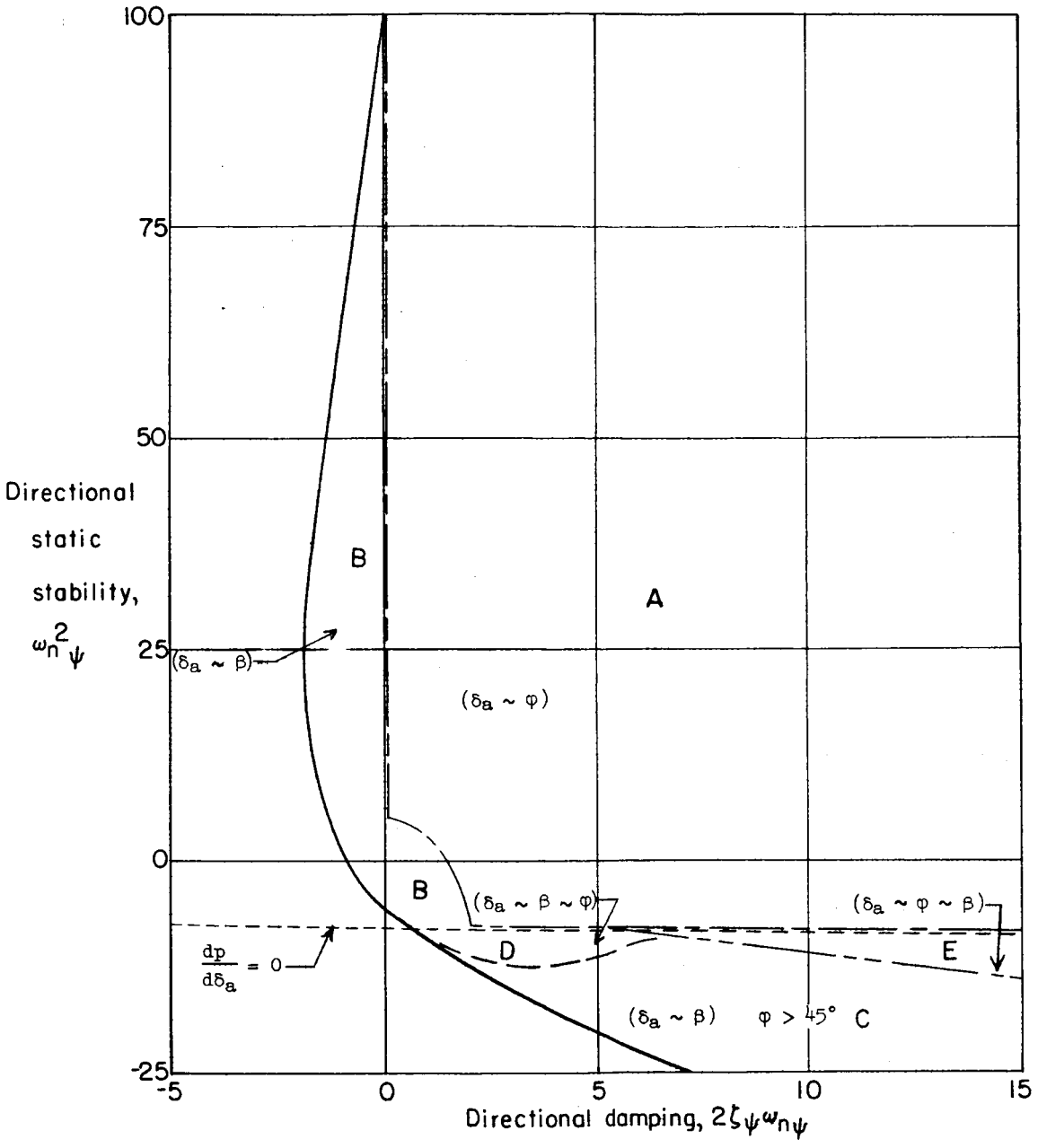

Figure 10.- Lateral-directional controllability limits using ailerons only.

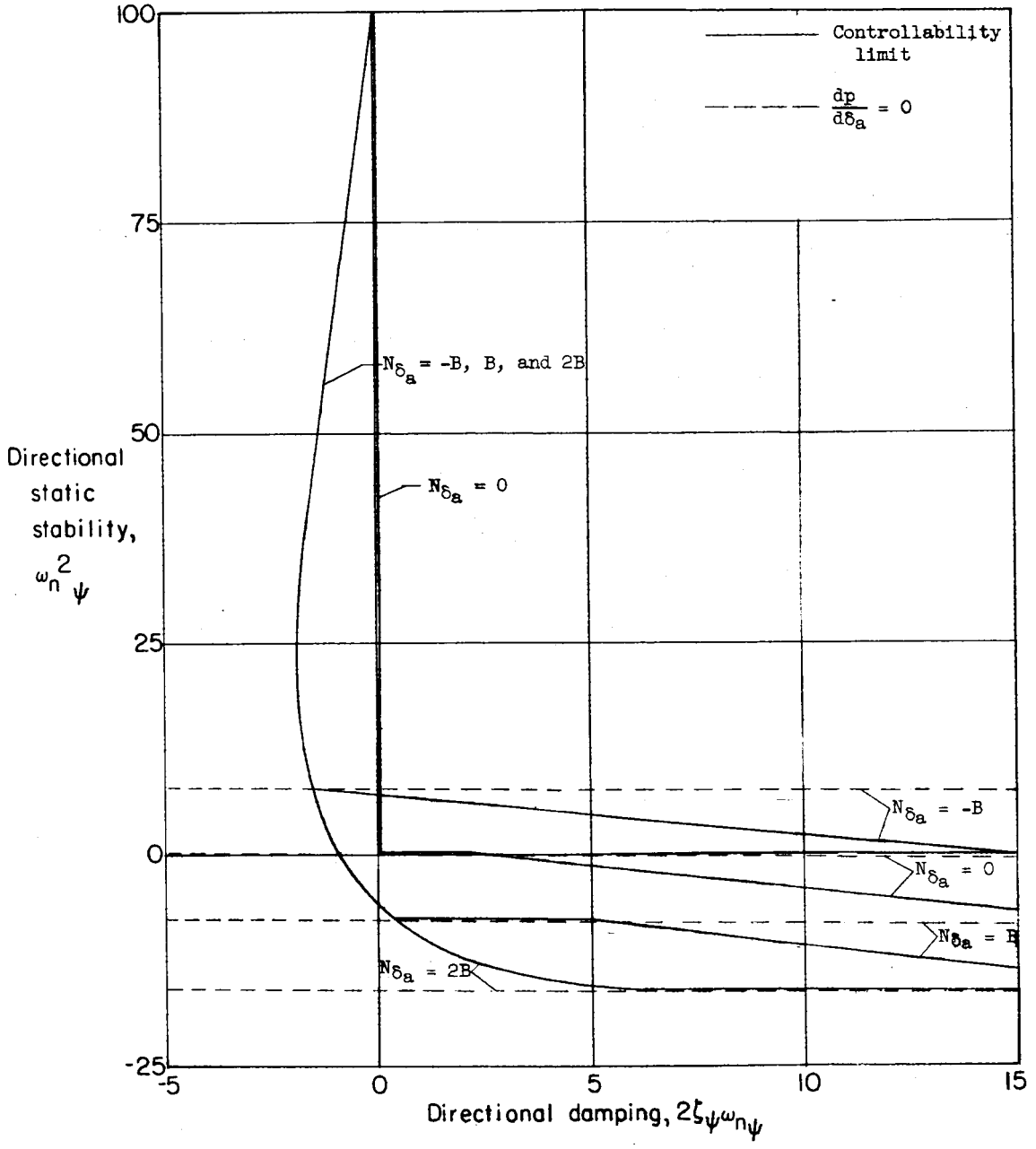

Figure 11.- Effect of yawing moment due to aileron deflection on the lateral-directional controllability limit.

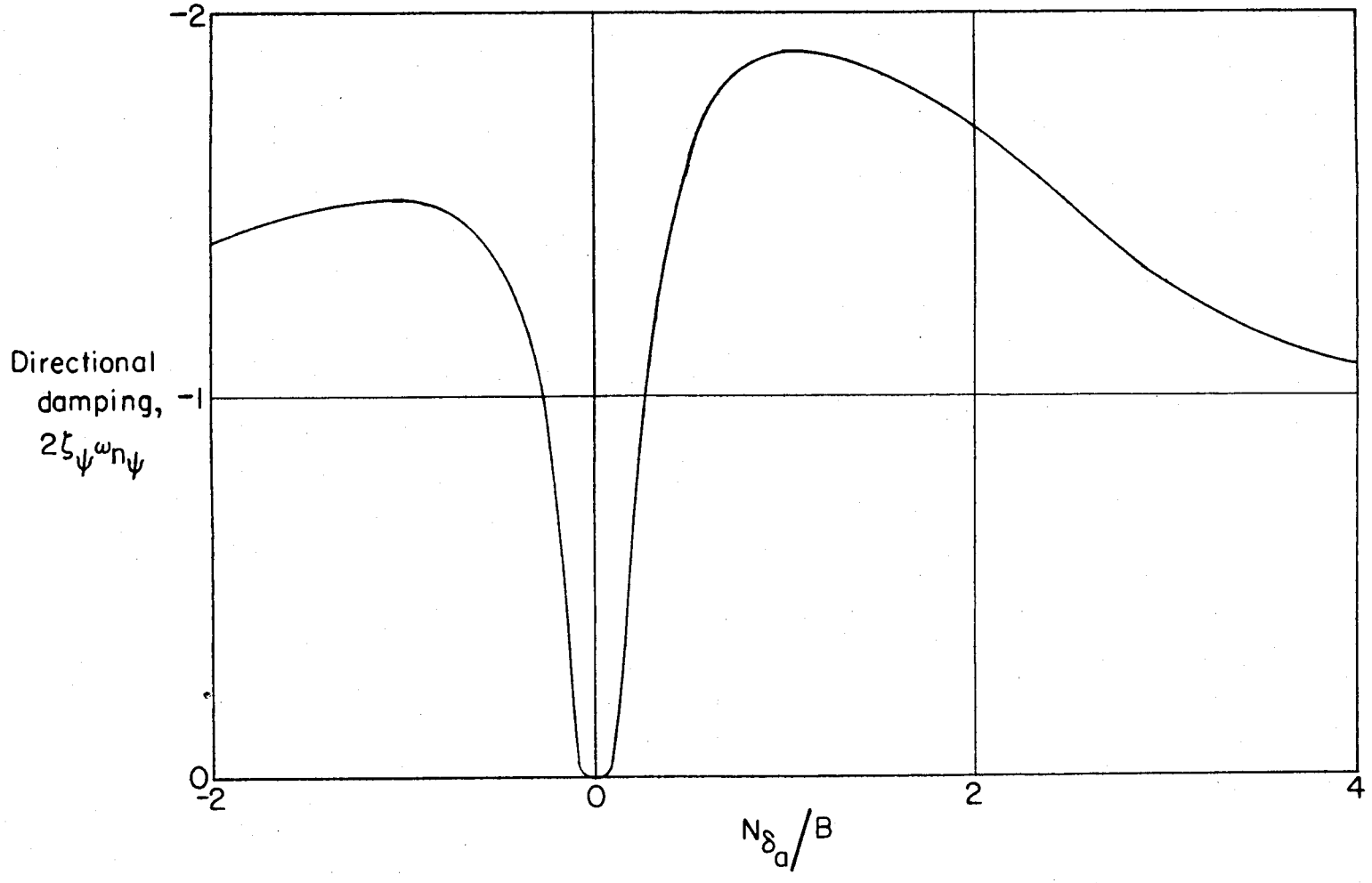

Figure 12.- Effect of yawing moment due to aileron deflection N_{δ_a} on the level of controllable dynamic instability. $\omega_n^2 = 15.6$.

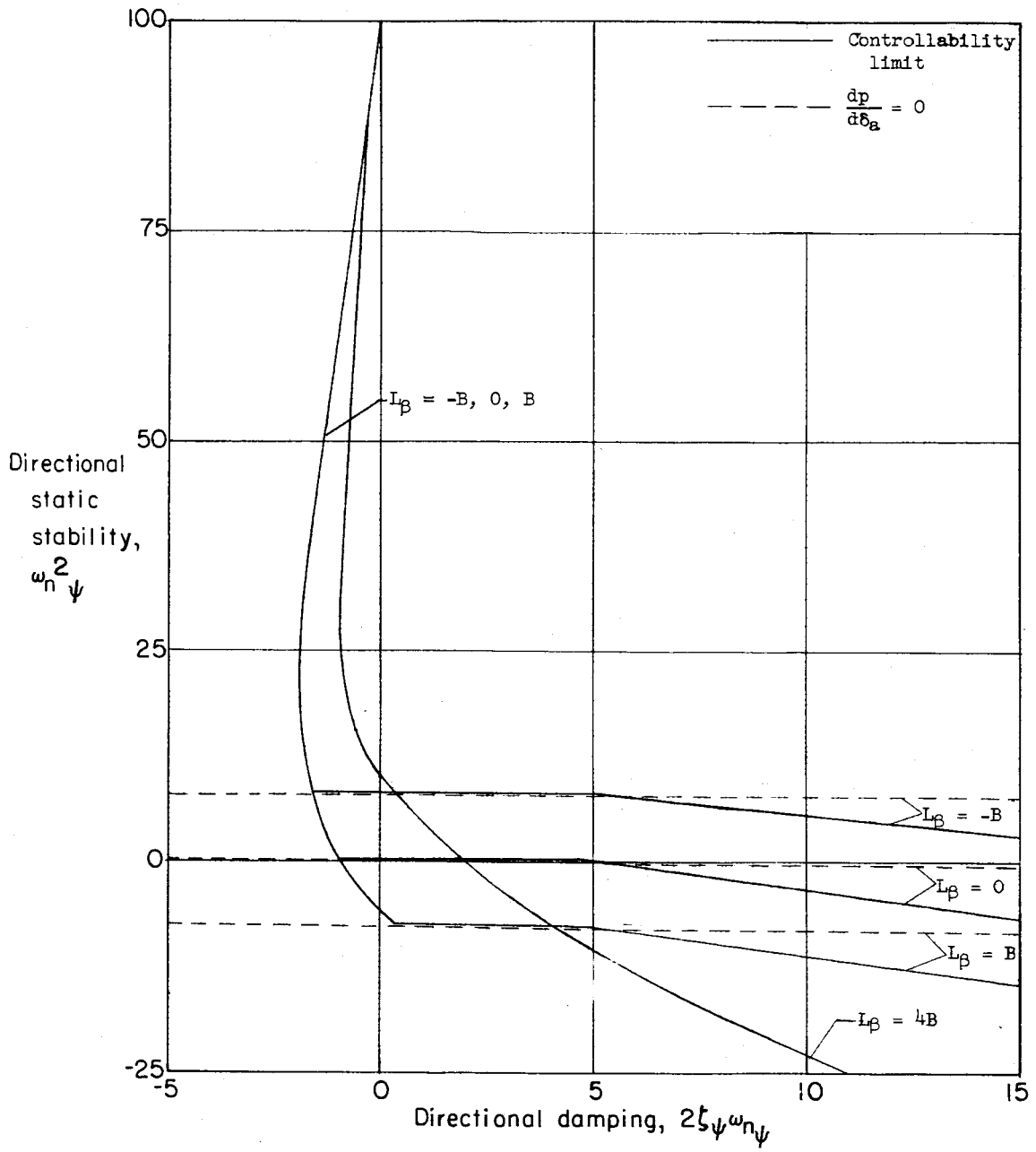

Figure 13.- Effect of L_β on the lateral-directional controllability limit when using ailerons only.

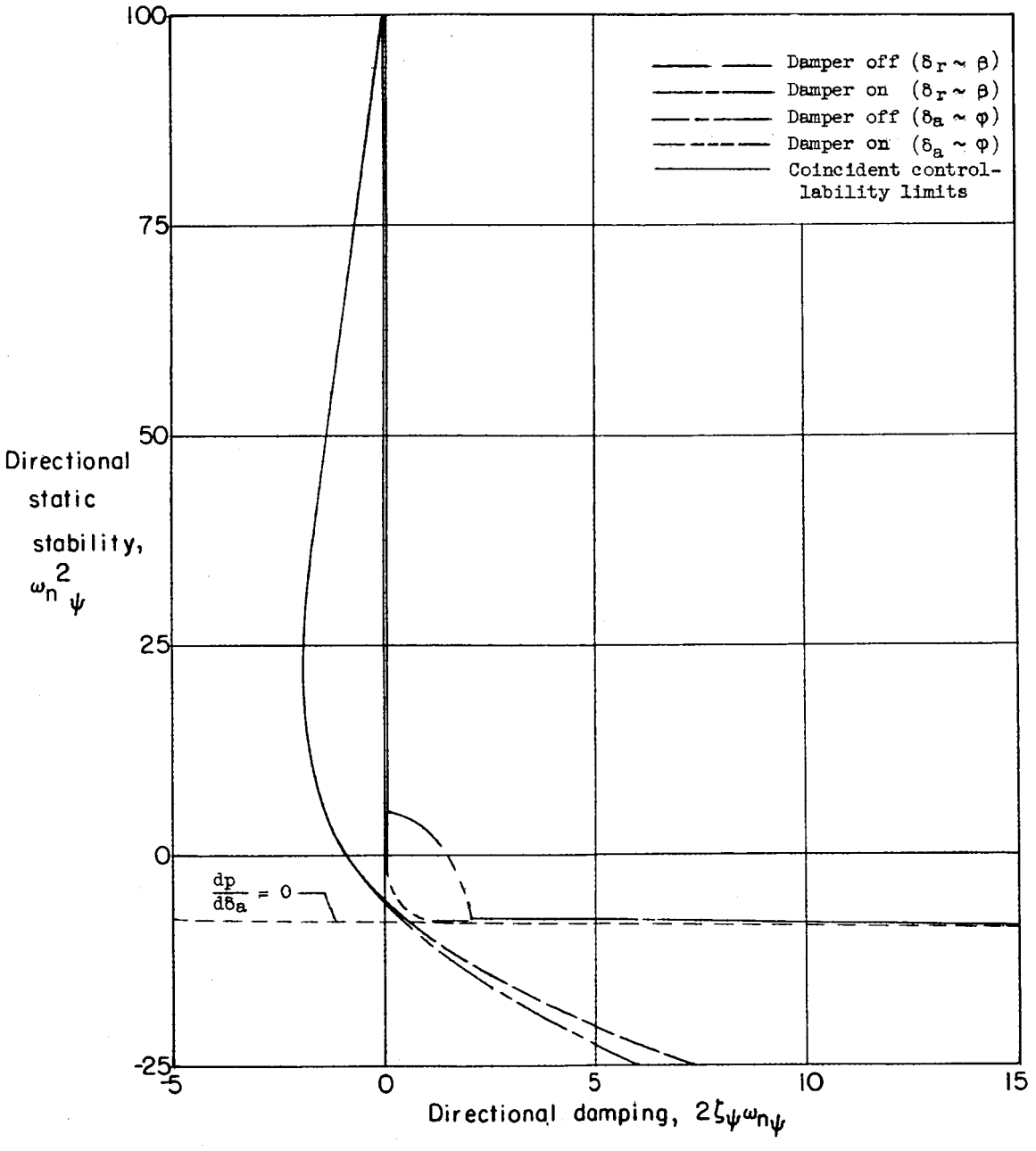

Figure 14.- Effect of a roll damper on the lateral-directional controllability limit.

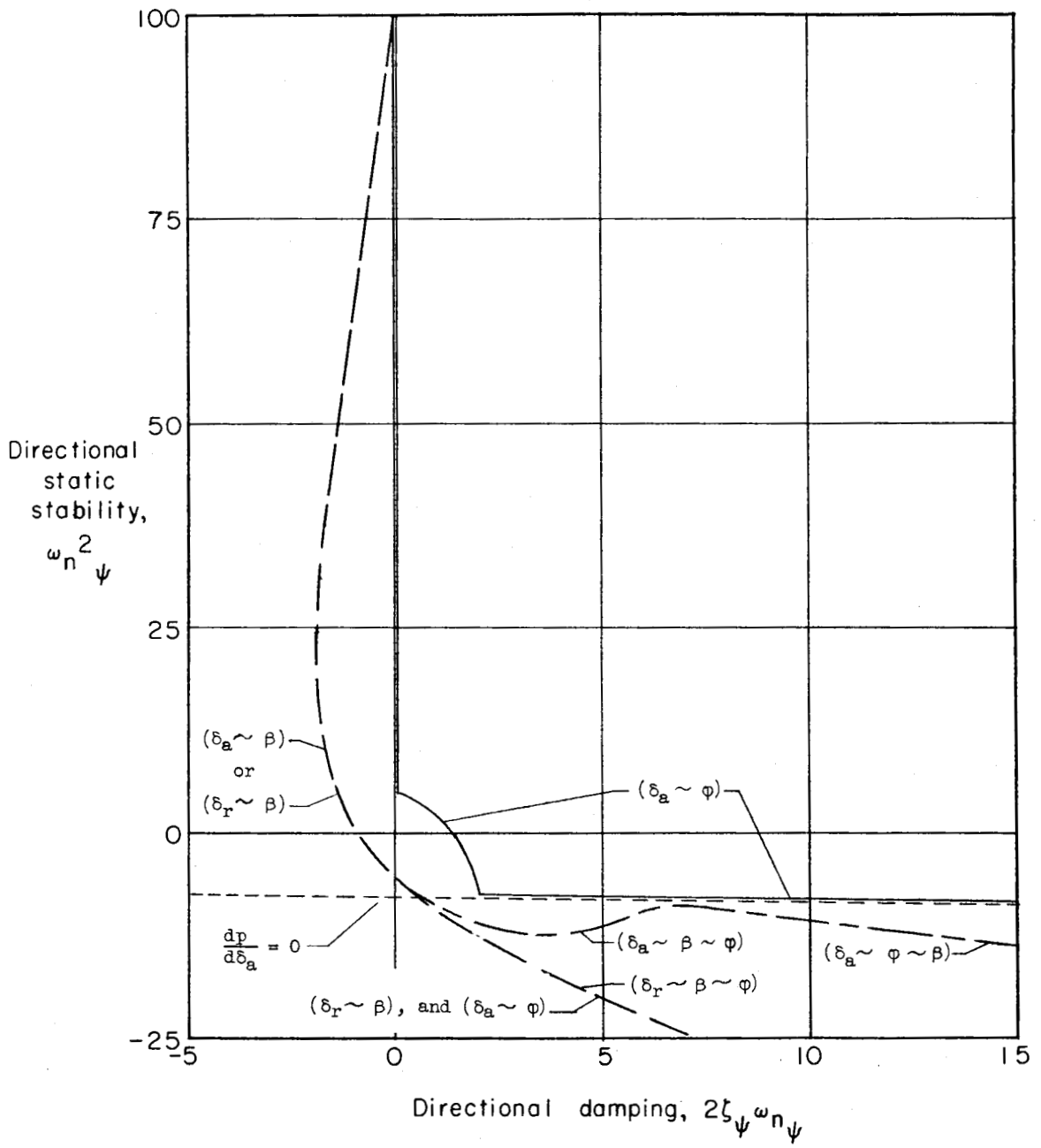

Figure 15.- Comparison of lateral-directional controllability limits determined from fixed-base-simulator tests.

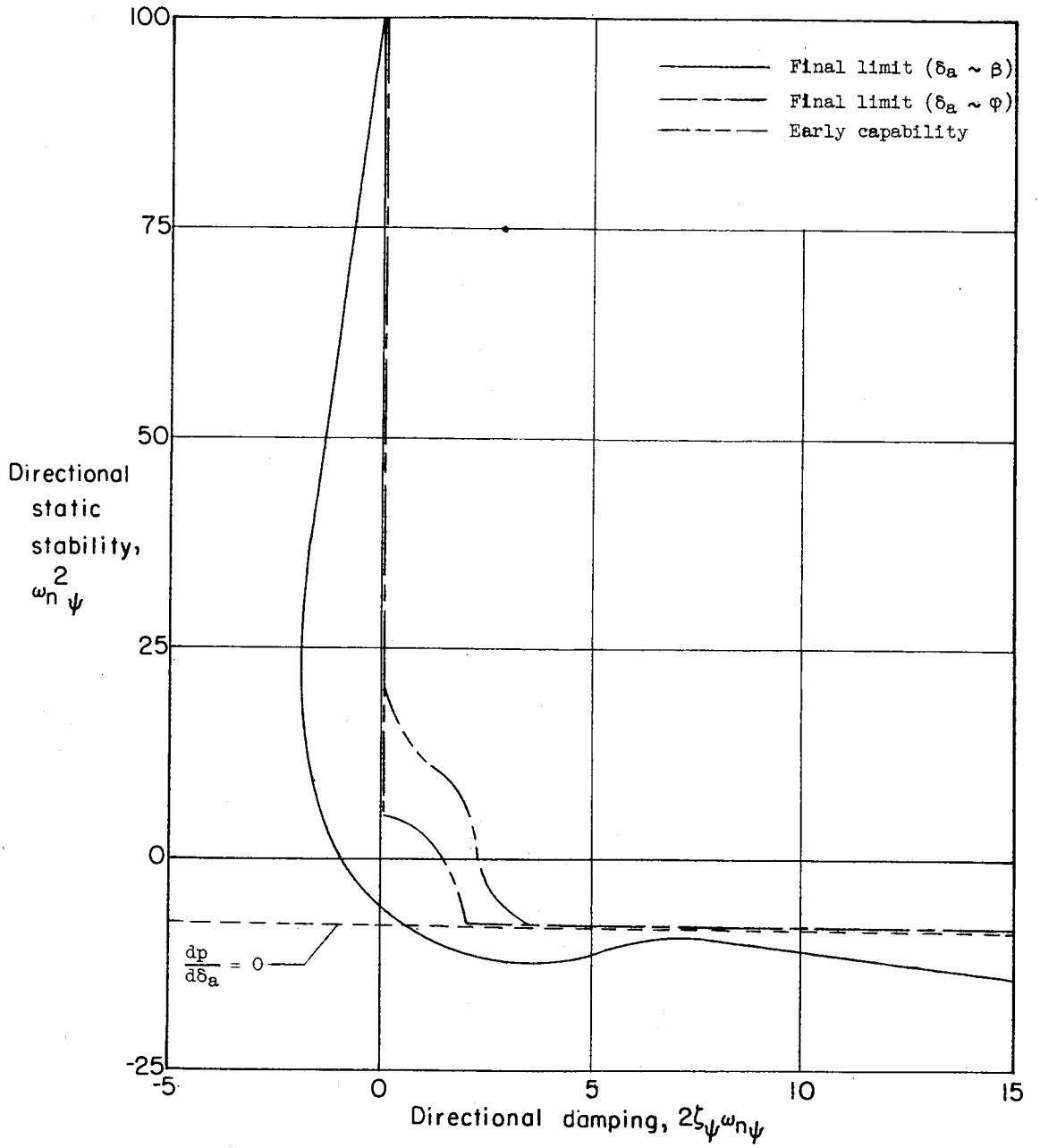

Figure 16.- Effect of pilot learning on the lateral-directional controllability limit when using ailerons only.

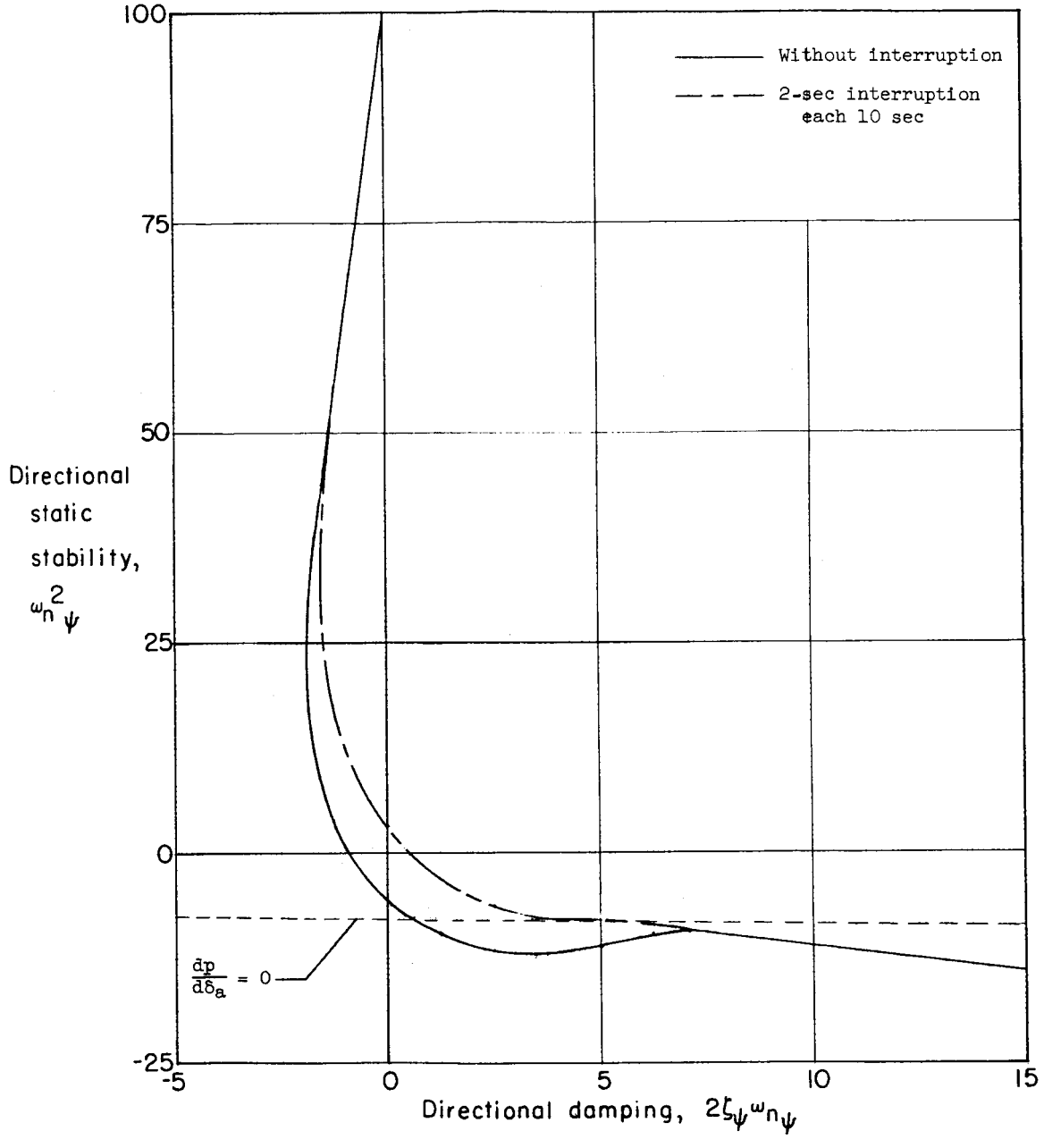

Figure 17.- Effect of a periodic 2-second interruption on the lateral-directional controllability limit when ailerons only are used.

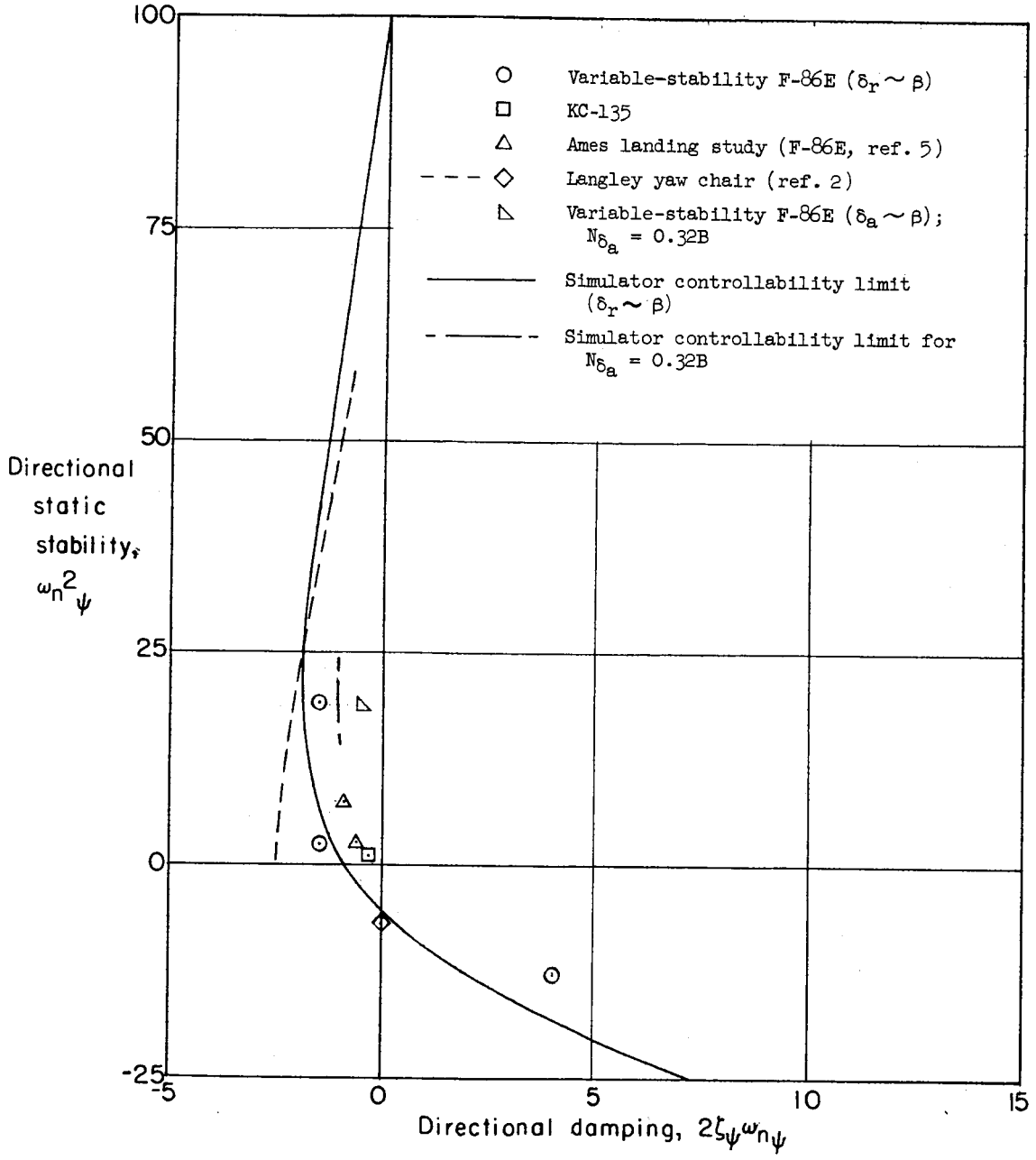

Figure 18.- Comparison of lateral-directional controllability limit with flight-test and yaw-chair results.

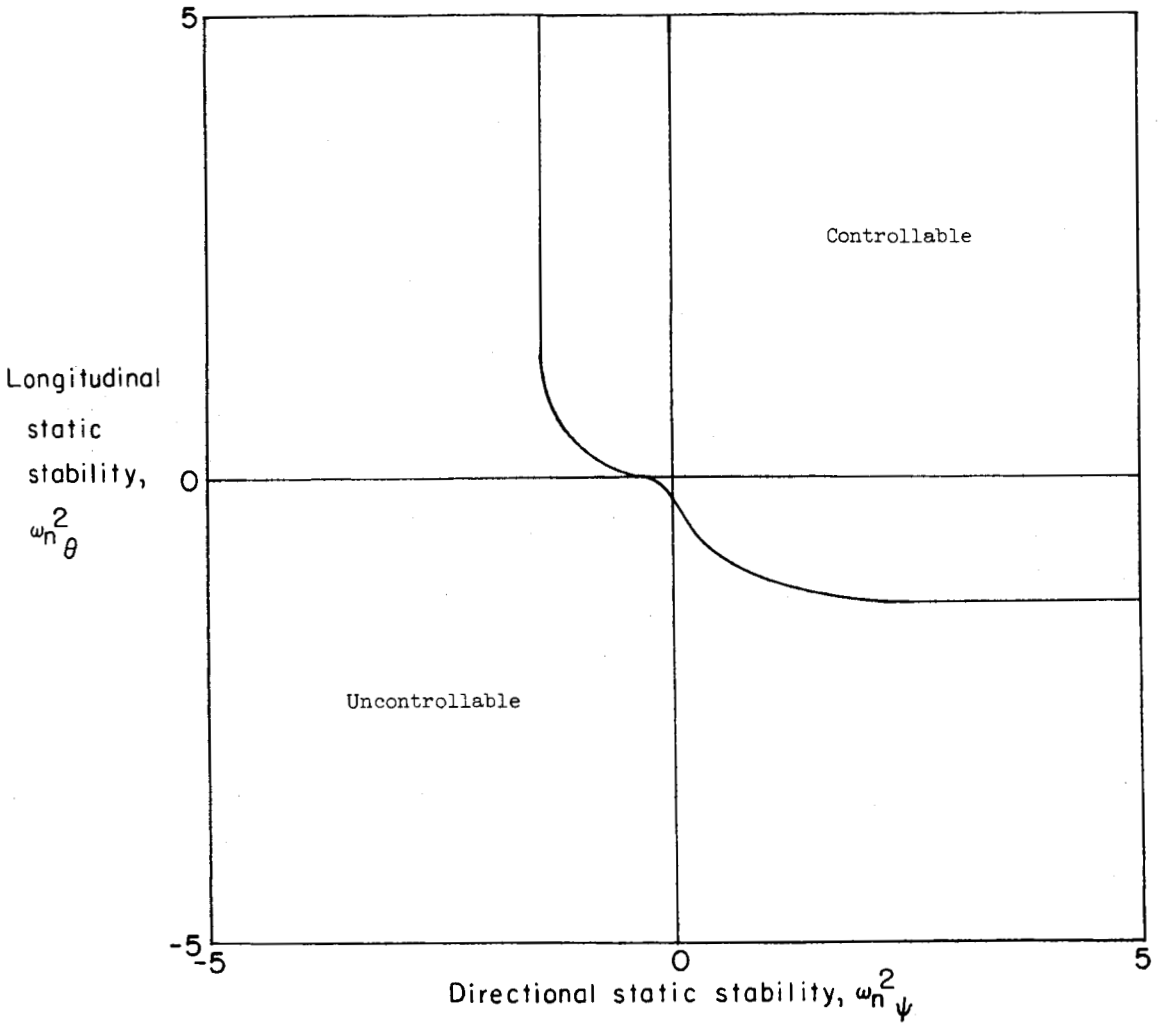

Figure 19.- A controllability limit as a function of the longitudinal and directional static stability. Longitudinal and directional damping at their basic values. ($\delta_a \sim \beta$).

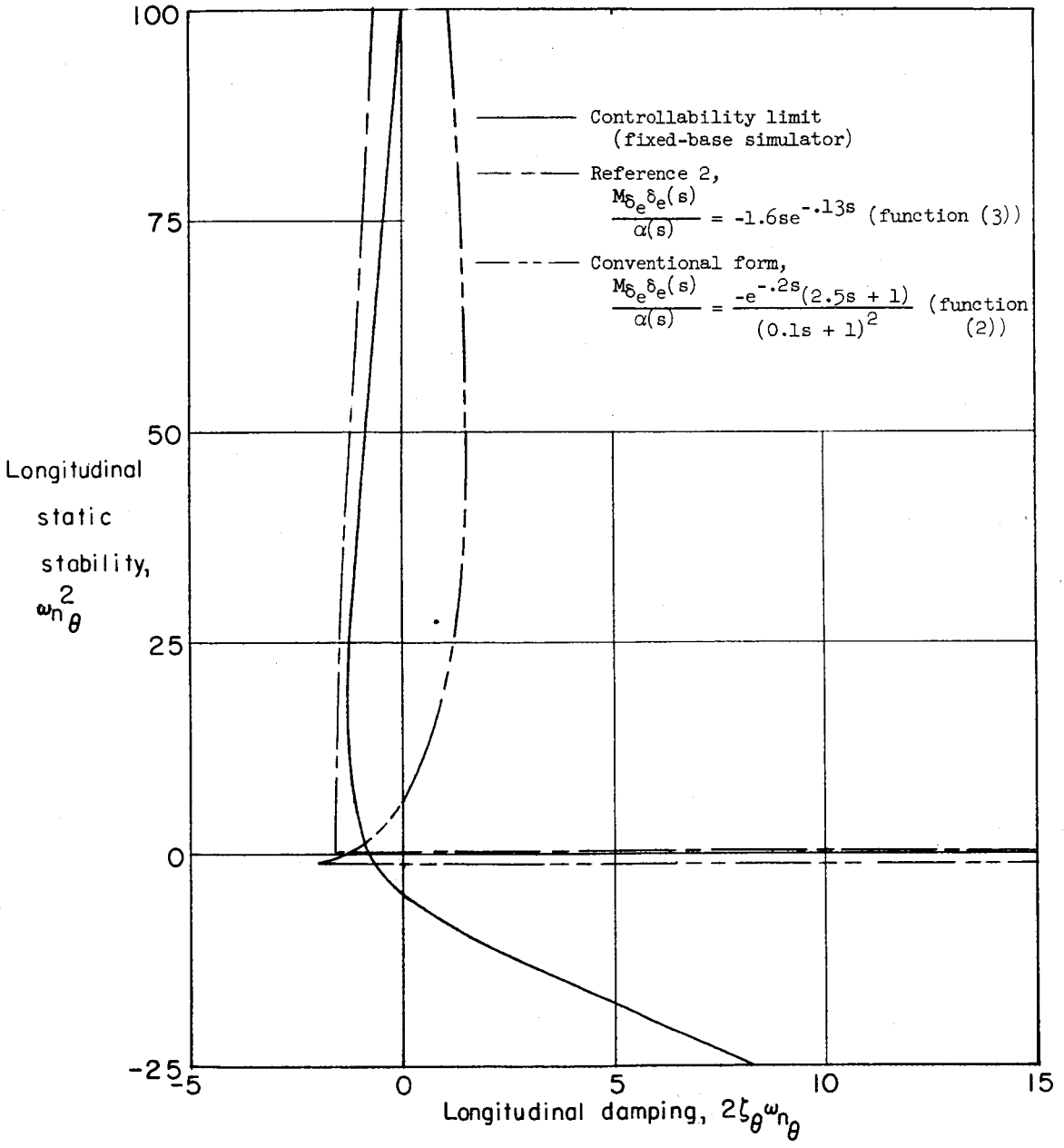

Figure 20.- Comparison of areas indicated to be controllable by using two different human transfer functions with the area found to be controllable in the fixed-base-simulator study.

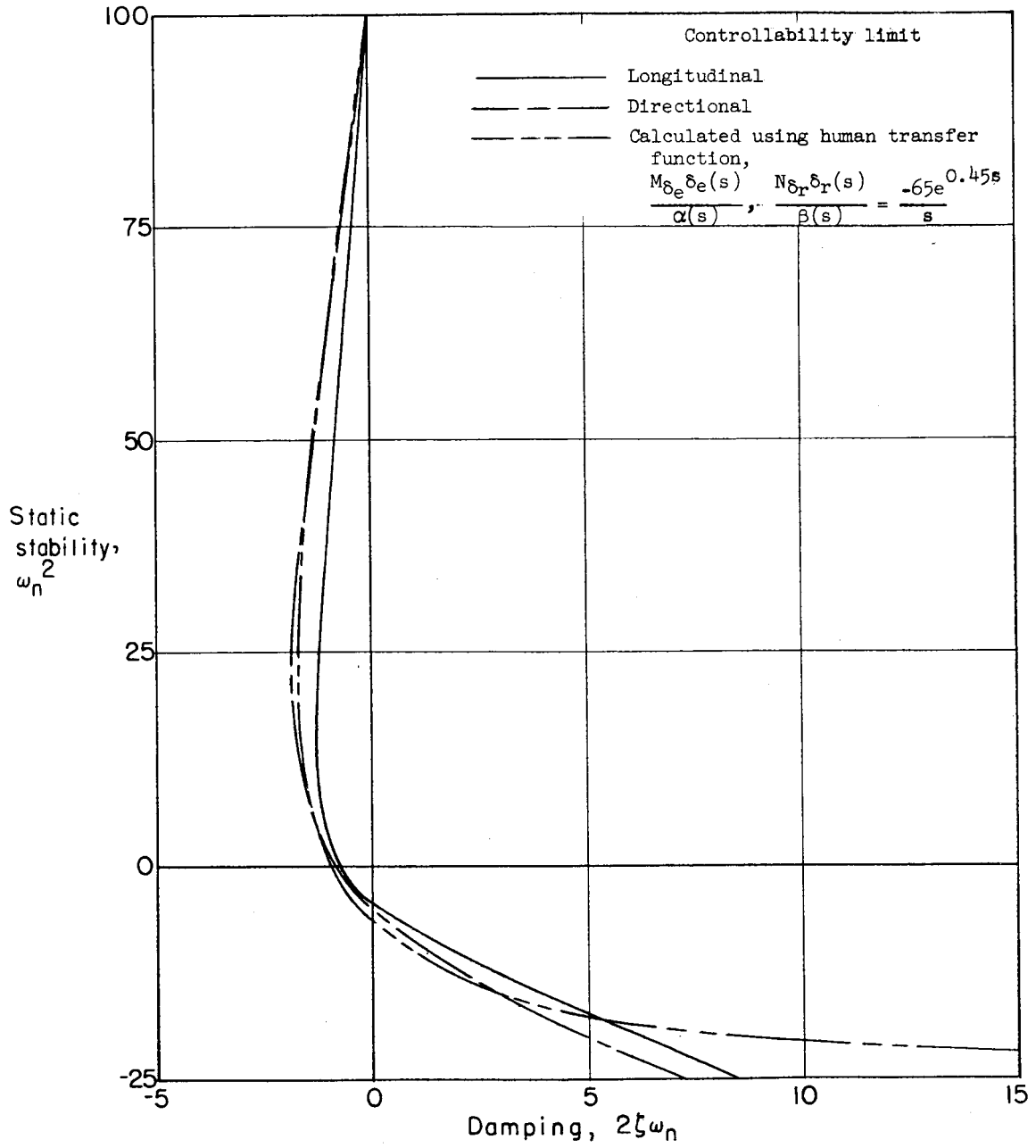

Figure 21.- Comparison of area indicated to be controllable by using a human transfer function with the area found to be controllable in the fixed-base-simulator study.

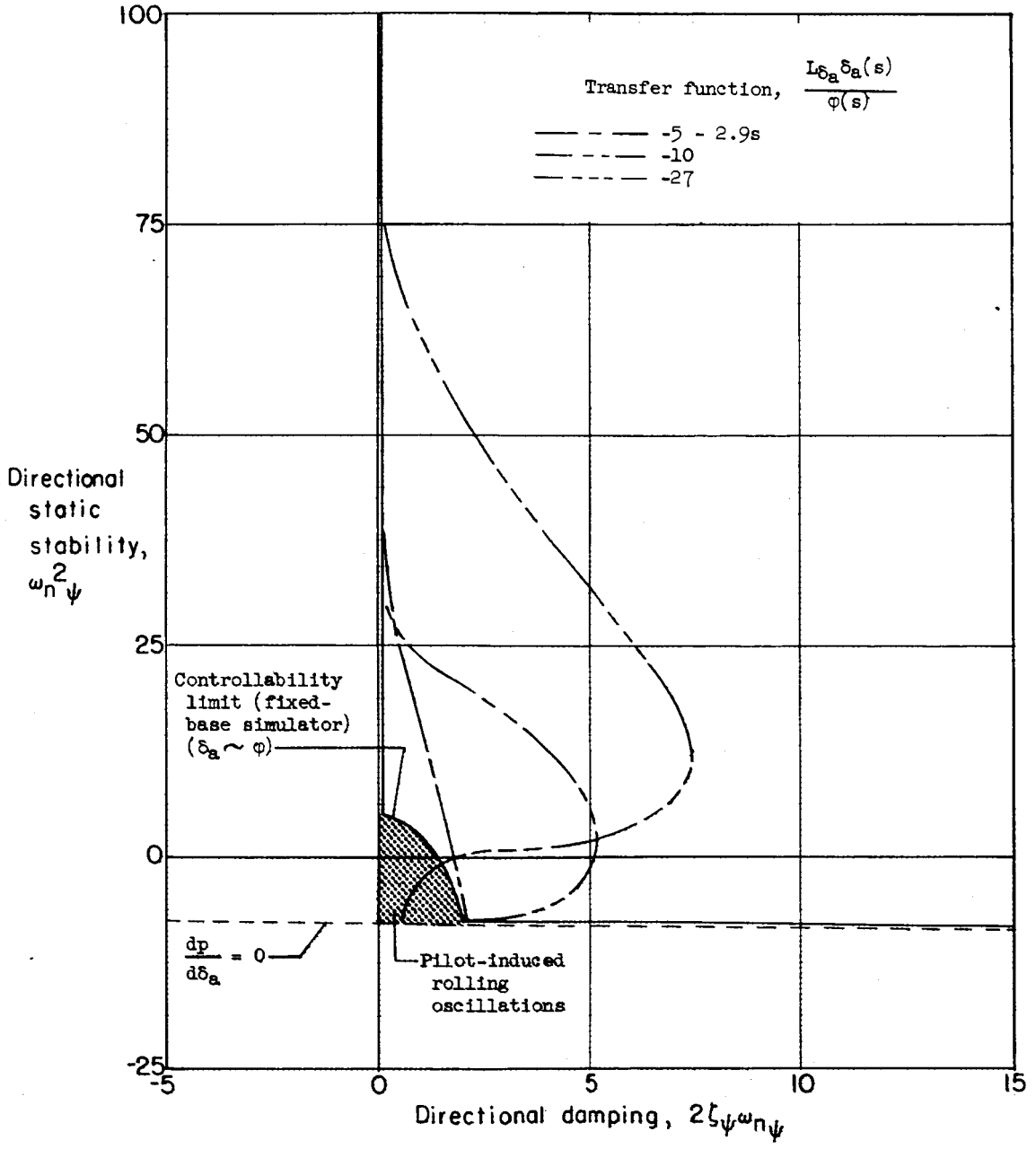

Figure 22.- Comparison of the controllability limit of bank-angle control with several limits calculated by using various human transfer functions.

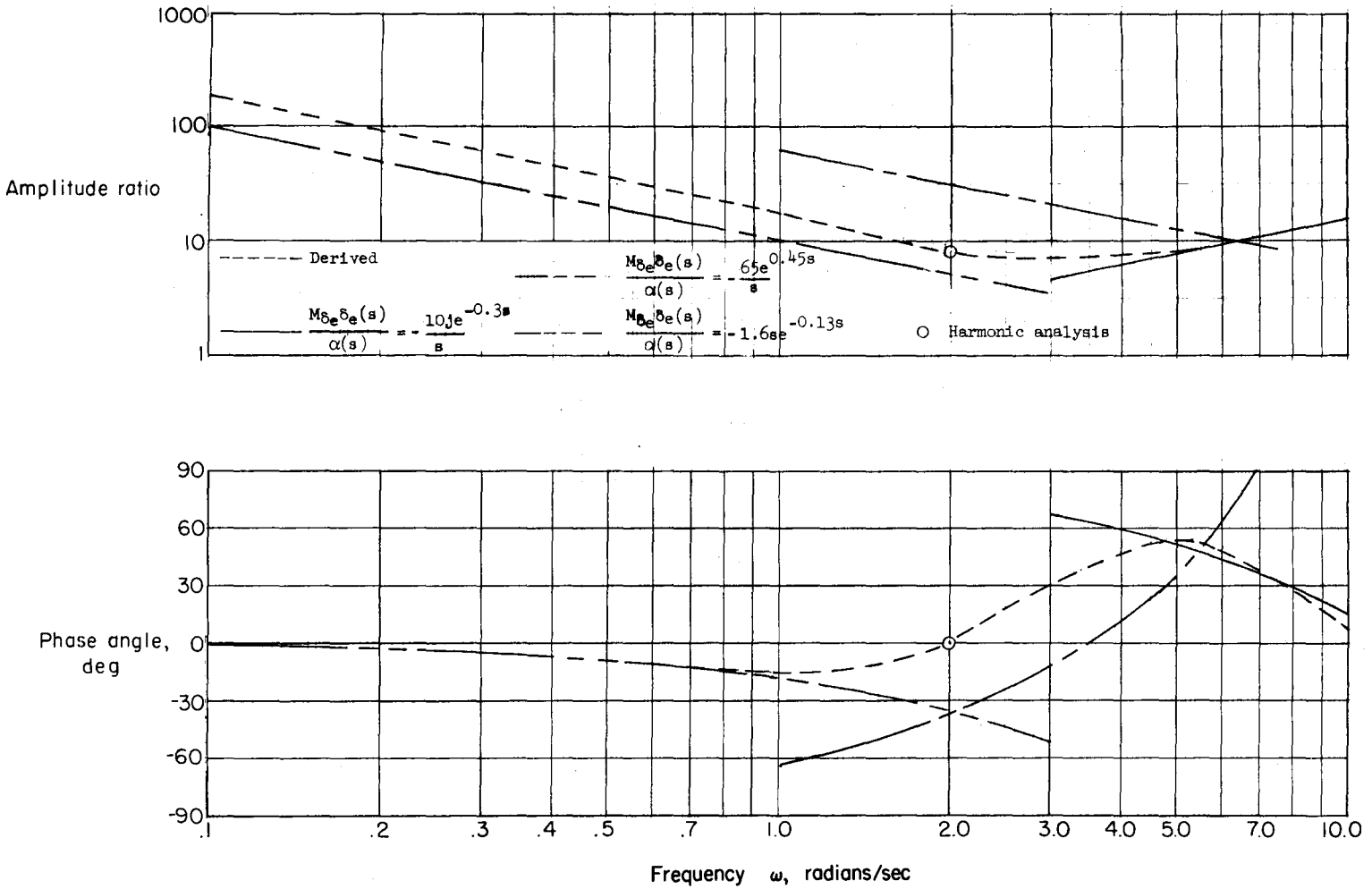

Figure 23.- Human transfer functions compared to the transfer function derived by using the controllability limit.

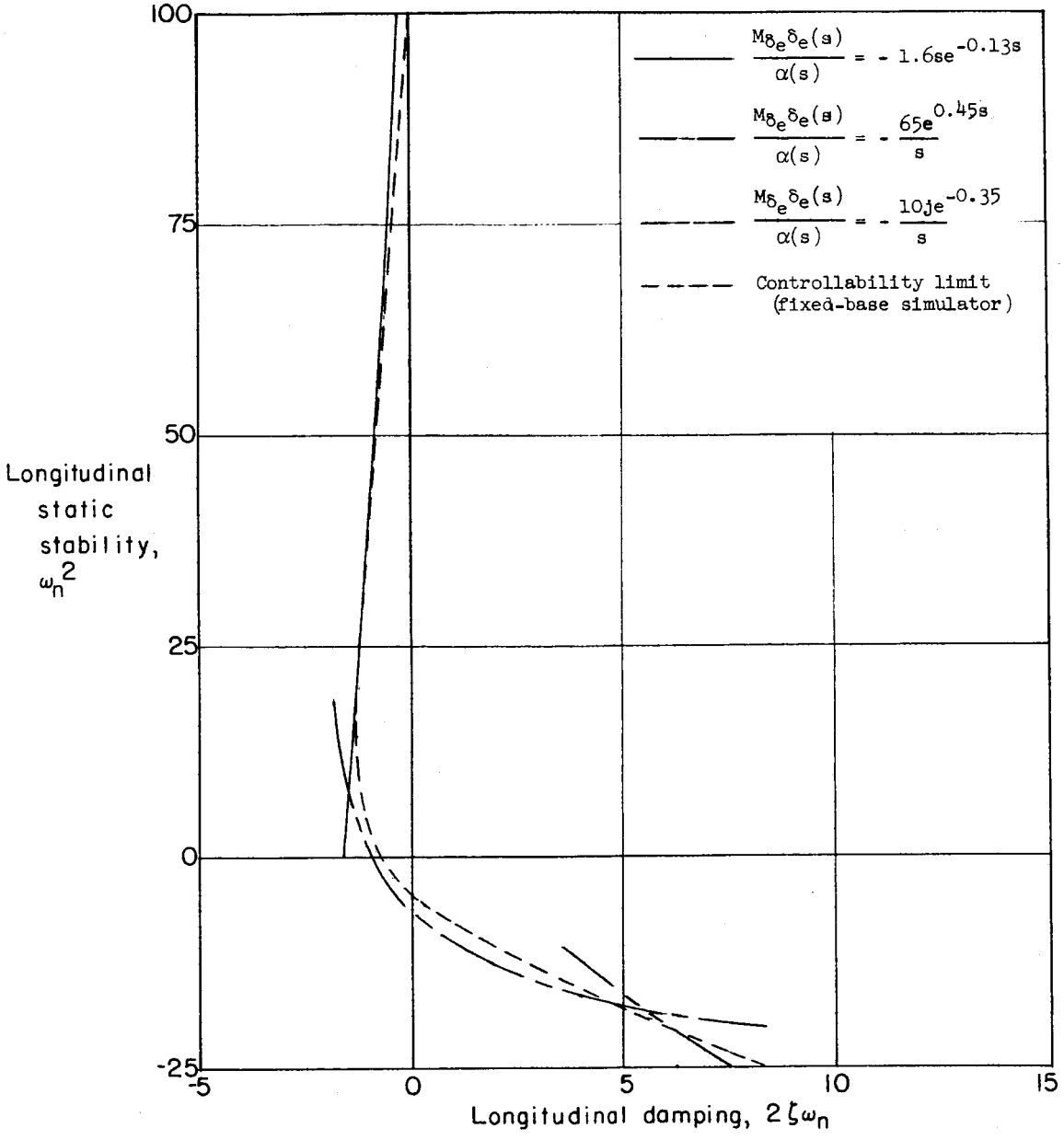

Figure 24.- Controllability limits calculated by using three human transfer functions.